Title

Identification of the binding sites for ubiquinone and inhibitors in the Na+-pumping NADH-ubiquinone oxidoreductase from Vibrio cholerae by photoaffinity labeling

Journal

Journal of Biological Chemistry, 292(19)

ISSN

0021-9258

Authors

Ito, Takeshi
Murai, Masatoshi
Ninokura, Satoshi
et al.

Publication Date

2017-05-01

DOI

10.1074/jbc.m117.781393

Peer reviewed

Identification of the binding sites for ubiquinone and inhibitors in the Na^+-pumping NADH-ubiquinone oxidoreductase from *Vibrio cholerae* by photoaffinity labeling

Received for publication, February 14, 2017, and in revised form, March 11, 2017 Published, Papers in Press, March 15, 2017, DOI 10.1074/jbc.M117.781393

Takeshi Ito[‡], Masatoshi Murai[‡], Satoshi Ninokura[‡], Yuki Kitazumi[‡], Katherine G. Mezic[§¶], Brady F. Cress[¶‖], Mattheos A. G. Koffas[§¶‖], Joel E. Morgan[¶], Blanca Barquera[§¶], and Hideto Miyoshi[‡1]

From the [‡]Division of Applied Life Sciences, Graduate School of Agriculture, Kyoto University, Sakyo-ku, Kyoto 606-8502, Japan and the Departments of [§]Biological Sciences and [‖]Chemical and Biological Engineering, [¶]Center for Biotechnology and Interdisciplinary Studies, Rensselaer Polytechnic Institute, Troy, New York 12180

Edited by Ruma Banerjee

The Na^+-pumping NADH-quinone oxidoreductase (Na^+-NQR) is the first enzyme of the respiratory chain and the main ion transporter in many marine and pathogenic bacteria, including *Vibrio cholerae*. The *V. cholerae* Na^+-NQR has been extensively studied, but its binding sites for ubiquinone and inhibitors remain controversial. Here, using a photoreactive ubiquinone PUQ-3 as well as two aurachin-type inhibitors [^{125}I]PAD-1 and [^{125}I]PAD-2 and photoaffinity labeling experiments on the isolated enzyme, we demonstrate that the ubiquinone ring binds to the NqrA subunit in the regions Leu-32–Met-39 and Phe-131–Lys-138, encompassing the rear wall of a predicted ubiquinone-binding cavity. The quinolone ring and alkyl side chain of aurachin bound to the NqrB subunit in the regions Arg-43–Lys-54 and Trp-23–Gly-89, respectively. These results indicate that the binding sites for ubiquinone and aurachin-type inhibitors are in close proximity but do not overlap one another. Unexpectedly, although the inhibitory effects of PAD-1 and PAD-2 were almost completely abolished by certain mutations in NqrB (*i.e.* G140A and E144C), the binding reactivities of [^{125}I]PAD-1 and [^{125}I]PAD-2 to the mutated enzymes were unchanged compared with those of the wild-type enzyme. We also found that photoaffinity labeling by [^{125}I]PAD-1 and [^{125}I]PAD-2, rather than being competitively suppressed in the presence of other inhibitors, is enhanced under some experimental conditions. To explain these apparently paradoxical results, we propose models for the catalytic reaction of Na^+-NQR and its interactions with inhibitors on the basis of the biochemical and biophysical results reported here and in previous work.

The Na^+-pumping NADH-quinone oxidoreductase (Na^+-NQR)[2] is the first enzyme of the respiratory chain and the main ion transporter in many marine and pathogenic bacteria, such as *Vibrio cholerae* and *Haemophilus influenzae* (1, 2). Na^+-NQR obtains energy by oxidizing NADH and reducing ubiquinone, which allows it to generate an electrochemical Na^+ gradient across the inner bacterial membrane. The enzyme is an integral membrane complex consisting of six subunits (NqrA–F) encoded by the *nqr* operon (2). There is a consensus that the electron transfer takes place through a series of five redox cofactors as follows: a FAD; a 2Fe-2S center; two covalently bound FMN, and a riboflavin (3–5). Different studies have intensively investigated the locations and redox properties of the cofactors of the enzyme (6–12); however, the exact locations of the ubiquinone-binding site(s) and the Na^+ transport pathway, as well as the mechanism that couples Na^+ transport to the electron transfer, still remain elusive.

A recently published X-ray crystallographic study provided important information about the structure of *V. cholerae* Na^+-NQR (13), but the model includes several features that are difficult to reconcile with previous biochemical and/or biophysical functional characterizations (11). For instance, the spatial distances between several pairs of redox cofactors in the proposed electron transfer pathway are too large to support physiological rates of electron transfer; for example, the edge-to-edge distance between the [2Fe-2S] cluster in NqrF and the $Fe(Cys)_4$ in NqrD (33.4 Å) and between the FMN and the riboflavin cofactor in NqrB (29.3 Å). The fact that electron transfer between these cofactors takes place indicates that the subunits harboring the cofactors undergo large conformational changes during turnover that decrease these spatial gaps (13).

Additionally, the crystallographic model lacks an anticipated tightly bound quinone, which has been reported in the enzyme preparations from different laboratories (4, 6, 8) and suggested to be located in NqrA on the basis of photoaffinity labeling and NMR studies (7, 9). In the crystallographic model, the NqrA subunit includes a deep cavity that is large enough to accommodate a ubiquinone molecule, but the cavity is ~20 Å above the predicted membrane surface and the distance between the cavity and the riboflavin in NqrB subunit is too large (>40 Å) to be consistent with electron transfer during turnover (Fig. 1).

This work was supported by Grants-in-aid for Scientific Research 26292060 (to H. M.), 15K07411 (to M. M.), and 16J02535 (to T. I.) from the Japan Society for the Promotion of Science. The authors declare that they have no conflicts of interest with the contents of this article.
This article was selected as one of our Editors' Picks.
This article contains supplemental data, Schemes S1–S5, and additional references.

[1] To whom correspondence should be addressed. Tel.: 81-75-753-6119; E-mail: miyoshi@kais.kyoto-u.ac.jp.

[2] The abbreviations used are: Na^+-NQR, Na^+-pumping NADH-quinone oxidoreductase; CBB, Coomassie Brilliant Blue R-250; Q_1, ubiquinone-1; Q_2, ubiquinone-2; LDAO, lauryldimethylamine *N*-oxide; DDM, dodecyl maltoside; TAMRA, 6-carboxy-*N,N,N′,N′*-tetramethylrhodamine; HQNO, 2-*n*-heptyl-4-hydroxyquinoline *N*-oxide.

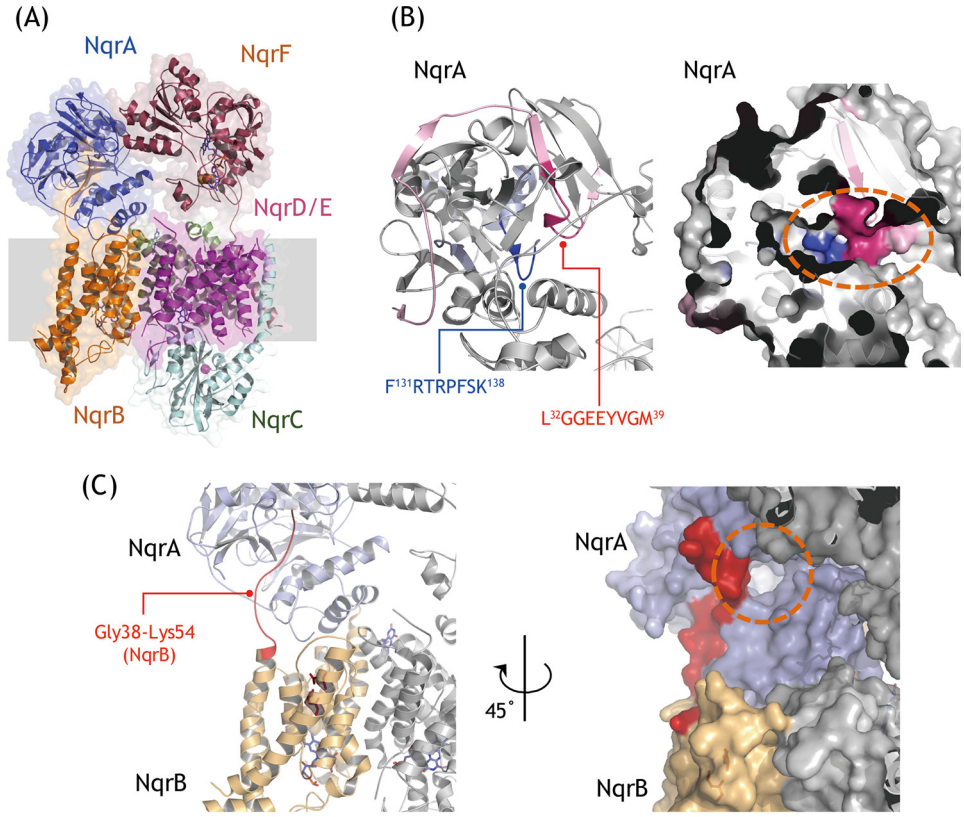

Figure 1. X-ray crystallographic model of Na^+-NQR and the location of the binding locations of ubiquinone and inhibitor. *A,* entire structure of *V. cholerae* Na^+-NQR (Protein Data Bank code 4P6V). *B,* close-up view of the binding location of PUQ-3 in the NqrA subunit. The structure is presented as both *ribbon* and *surface* models. The predominant (Ile-2–Met-39 in *light* and *deep red*) and subsidiary (Val-94–Met-154 in *light* and *deep blue*) labeled regions are shown. Ile-2–Leu-30 (*light red*) and Val-94–Phe-130 (*light blue*) can be ruled out as candidates for the binding location of the ubiquinone ring, as discussed in the text. The putative solvent-accessible cavity is marked by a *dashed orange oval. C,* close-up view of the binding location of inhibitor in the NqrB subunit. The structures are presented as both *ribbon* and *surface* models. The region Gly-38–Lys-54 is shown in *red*. An N-terminal stretch Met-1–Pro-37 was not modeled in Ref. 13. The *dashed orange circle* marks an entrance to the putative ubiquinone-binding cavity. The amino acids corresponding to the mutants (NqrB-Gly-140, -Gly-141, and -Glu-144) are shown as a *stick model* (*red*).

To understand the mechanistic details of respiratory enzymes that use the quinone/quinol molecule as a substrate, identification of the binding site for quinone/quinol at the amino acid level is critical. Recently, by alanine-scanning mutagenesis of aromatic residues in NqrB and molecular docking, Tuz *et al.* (14) proposed that the binding site of the ubiquinone ring is located at the interface of the NqrB and NqrD subunits. The predicted site is not only inconsistent with the location of the putative cavity in NqrA (13), but is also too far from the riboflavin (~36 Å) for efficient electron transfer. Because the work by Tuz *et al.* (14) was largely based on steady-state kinetic analysis of mutants, it is difficult to determine whether the critical residues that they identified (NqrB-Phe-211 and -Phe-213) are directly involved in forming the binding pocket for the ubiquinone ring or whether they affect the reaction of ubiquinone indirectly though some long-range conformational change. In addition, to determine the number of binding sites and/or the dissociation constant for short-chain ubiquinone and the inhibitor HQNO, previous studies employed the equilibrium dialysis method with isolated wild-type and mutated Na^+-NQR (10, 14). However, interpretation of data obtained through this method can be problematic because it may be impossible to distinguish between specific and non-specific binding of the hydrophobic ligands to the enzyme, particularly in the case of an integral membrane protein. Thus, there remains considerable controversy regarding the number and location of quinone-binding site(s) in Na^+-NQR.

As specific inhibitors of many respiratory enzymes disturb the enzyme function, in general, by interfering with the redox reaction of quinone/quinol, identification of the binding site for inhibitors is also invaluable. The inhibitors that have been used for previous Na^+-NQR research are limited to a few commercially available chemicals such as HQNO (8, 9), which has only moderate inhibitory potency (IC_{50} or K_i value in the micromolar range). Korormicin (Fig. 2), a natural antimicrobial produced by some marine bacteria, was reported by Hayashi *et al.* (15) to be a very potent inhibitor of Na^+-NQR from *V. cholerae* with a K_i about 3000-fold tighter than that of HQNO. On this basis, korormicin can be anticipated to be a useful molecular tool for Na^+-NQR research. However, it is no longer possible to acquire korormicin because the Japanese research institute, where it was originally isolated, has been closed. For this study, we made a fresh isolation of korormicin from culture broth of marine bacterium *Pseudoalteromonas* J010.

Additionally, through extensive screening of potential inhibitors of *V. cholerae* Na^+-NQR from the chemical library of our laboratory, we identified an aurachin derivative (aurachin D-42, Fig. 2) as a very effective inhibitor of the enzyme, with a potency almost identical to that of korormicin. With the two strong

inhibitors in hand, we have used a photoaffinity labeling technique to identify the binding sites for ubiquinone and aurachin-type inhibitors in isolated *V. cholerae* Na^+-NQR. We also investigated the mechanism of inhibition of aurachin derivatives using the mutated enzymes G140A, G141V, and E144C in the NqrB subunit, in which the effects of these inhibitors are significantly attenuated (8, 10, 15). Some of the current results were initially difficult to reconcile. For example, there are two mutants in transmembrane helix II of the NqrB subunit (G140A and E144C), in which aurachin derivatives lose almost all inhibitory potency, even though the effectiveness of labeling to the mutated enzymes is essentially unchanged compared with the wild-type enzyme. In an attempt to explain these apparently paradoxical results, we propose models for the catalytic reaction of Na^+-NQR and the interaction with inhibitor on the basis of the biochemical and biophysical information obtained in this study and previous works.

Results

Korormicin and aurachin D-42

Korormicin was isolated from the culture broth of the marine bacterium *Pseudoalteromonas* strain J010 according to the method originally described by Yoshikawa *et al.* (16). The spectra of our isolated sample completely match those reported previously (16, 17), as described under "Experimental procedures." Aurachin D-42 was identified as a very effective inhibitor of *V. cholerae* Na^+-NQR from the chemical library of our laboratory. The inhibitory potencies of korormicin and aurachin D-42 were examined against the NADH-Q_1 oxidoreductase activity of Na^+-NQR using the isolated enzyme (0.9 nM) and measuring the reduction of quinone at 282 nm. The IC_{50} values of korormicin and aurachin D-42 were 5.0 (± 0.7) and 2.0 (± 0.3) nM, respectively. Thus, korormicin and aurachin D-42 are both ~1000-fold more potent than commercially available HQNO (an aurachin C-type analog), which has been widely used in previous studies (8, 15).

Design of photoreactive ubiquinone and aurachin derivatives

We have synthesized several photoreactive ubiquinone derivatives for previous photoaffinity labeling studies for other membrane proteins (18–20). However, a preliminary test of these derivatives showed that all are poor electron acceptors for *V. cholerae* Na^+-NQR with catalytic efficiencies ~15–30% that of Q_1. Therefore, we newly synthesized PUQ-3, which has a shorter side chain compared with the previous ubiquinone derivatives. An alkyne group (–C≡CH) was attached to the terminal end of the side chain to allow the conjugation of molecular tags, such as fluorophores and biotin, via Cu^+-catalyzed click chemistry (*i.e.* azide-alkyne [3+2] cycloaddition in water (21)) to detect the labeled peptide. PUQ-3 turned out to be an efficient electron acceptor for Na^+-NQR with K_m and V_{max} values of 8.3 (± 0.2) μM and 14.8 (± 1.9) μmol/min/mg of protein, respectively. Under the same experimental conditions, the K_m and V_{max} values of Q_1 were 8.3 (± 0.3) μM and 24.3 (± 3.1) μmol/min/mg of protein, respectively.

Next, we synthesized two photoreactive aurachin derivatives using aurachin D-42 as a molecular template (PAD-1 and PAD-2, see Fig. 2). Both derivatives incorporate photoreactive azido (–N=N^+=N^-) groups; the azido group is on the quinolone ring in PAD-1, although it is attached to the side chain moiety in PAD-2. Introduction of radioactive ^{125}I label into the two derivatives ([^{125}I]PAD-1 and [^{125}I]PAD-2) makes it possible to work with the lowest possible concentrations, thus minimizing the probability of non-specific labeling.

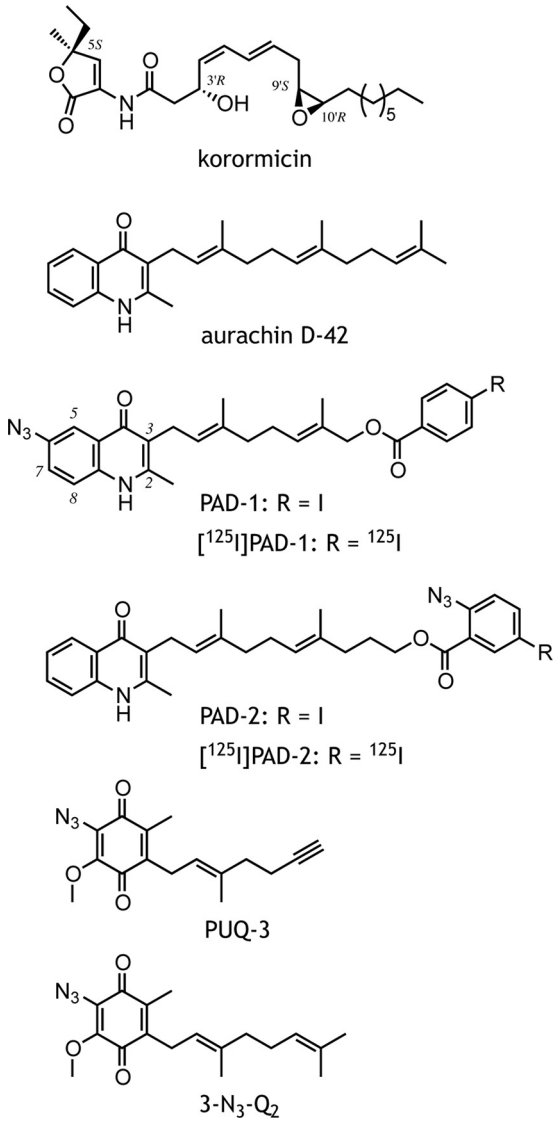

Figure 2. Structures of the test compounds used in this study: korormicin, aurachin D-42, PAD-1 (and [^{125}I]PAD-1), PAD-2 (and [^{125}I]PAD-2), PUQ-3, and 3-N_3-Q_2.

The inhibitory activities of PAD-1 and PAD-2, in terms of IC_{50} value, were 590 (±45) and 1.6 (±0.21) nM, respectively. Thus, although PAD-2 retains the potency of the native aurachin, at the single digit nanomolar level, PAD-1 is significantly less effective, presumably because of steric hindrance at the toxophoric quinolone ring, arising from the presence of the azido group. We changed the substitution position of the azido group on the quinolone ring to the 5-, 7-, or 8-position; however, the inhibitory potency did not recover. Nevertheless, we included [^{125}I]PAD-1 in the photoaffinity labeling study because it is still a much stronger inhibitor than HQNO.

In the case of korormicin, our preliminary structure-activity studies revealed that the methyl/ethyl branch and OH group

located at the 5*S* and 3′*R* positions, respectively, are critical for inhibitory activity.[3] Because of these complications in structural factors, synthetic production of photoreactive korormicin derivatives, which maintain as much inhibitory potency as possible, is still ongoing in our laboratory.

Photoaffinity labeling of Na^+-NQR by PUQ-3

Na^+-NQR that has been purified using the non-ionic detergent dodecyl maltoside (DDM) is reported to contain tightly bound ubiquinone-8 (Q_8) in substoichiometric quantities that can be removed by washing the enzyme preparation with a buffer containing the zwitterionic detergent lauryldimethylamine *N*-oxide (LDAO) (7, 10). We used LDAO-washed Na^+-NQR throughout this study.

Na^+-NQR (0.9 μM) was incubated with PUQ-3 (5 μM) on ice, irradiated with a UV lamp, then denatured with 1% (w/v) SDS, and covalently conjugated with a fluorescent TAMRA-N_3 via Cu^+-catalyzed click chemistry. The resulting proteins were separated on a 15% Laemmli-type SDS gel containing 6.0 M urea. Under these analytical conditions, Na^+-NQR was separated into six bands corresponding to the six subunits of the enzyme (Fig. 3*A*). The two bands, which migrated to the region of ~50 kDa, were confirmed to be the hydrophilic NqrF subunit, as demonstrated by Western blotting using an antibody against the N-terminal His tag, and the hydrophilic NqrA subunit, as demonstrated by MALDI-TOF MS (13 peptides, 30% coverage). Two other bands, which appeared in the region of ~30 kDa, were determined to be the hydrophobic NqrB and NqrC subunits on the basis of their N-terminal amino acid sequences. As these subunits each carry one covalently bound FMN (Fig. 3*A*, *center*), the FMN-based fluorescence was used as a loading control for SDS-PAGE throughout this study (22, 23). Although the NqrD and NqrE subunits were invisible in this gel, they become visible by heavy staining (data not shown).

As shown in Fig. 3*A*, a major TAMRA fluorescence was observed at the band corresponding to the NqrA subunit at ~50 kDa. The fluorescence intensity incorporated into the NqrA subunit was reduced when labeling was carried out in the presence of an excess of Q_2 or 3-N_3-Q_2 (100 μM each, 20 molar-fold) (Fig. 3*B*), indicating specific binding of PUQ-3 to Na^+-NQR. The suppressive effects of aurachin D-42 and korormicin (10 μM each, 2 molar-fold) on the labeling were significantly smaller than those of the short-chain quinones (Fig. 3*B*), even though the binding affinities of the potent inhibitors are at least 2 orders of magnitude stronger than that of PUQ-3. It may be noted that the NqrB subunit was also labeled faintly, but this minor labeling of NqrB was not examined in further detail.

Localization of the labeled site by PUQ-3

To localize the binding site of PUQ-3 in the NqrA subunit, the labeled NqrA band was subjected to *in gel* partial digestion with V8-protease (Cleveland mapping). As shown in Fig. 4*A*, this partial digestion reproducibly gave a major fluorescent band at ~12 kDa (fragment A) containing the internal sequence

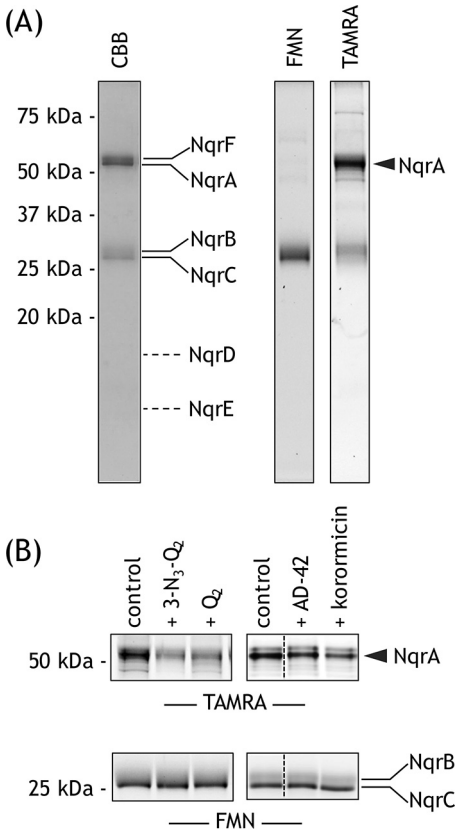

Figure 3. Photoaffinity labeling of Na^+-NQR by PUQ-3. *A,* LDAO-washed Na^+-NQR (0.9 μM) was incubated with PUQ-3 (5 μM), photoirradiated with a UV lamp, denatured with 1% (w/v) SDS, and conjugated with TAMRA-N_3 via Cu^+-catalyzed click chemistry. The proteins were resolved by a 15% Laemmli-type SDS gel containing 6.0 M urea and visualized by CBB stain or fluorescent imaging. *B,* LDAO-washed Na^+-NQR (0.9 μM) was labeled by PUQ-3 (5 μM) in the presence of an excess of 3-N_3-Q_2 (100 μM), Q_2 (100 μM), aurachin D-42 (10 μM), or korormicin (10 μM), followed by the conjugation with TAMRA-N_3 and SDS-PAGE. Approximately 3 μg of protein was loaded onto each lane. Data are representative of three independent experiments.

corresponding to Gly-7–Lys-24 of NqrA, (confirmed by MALDI-TOF MS, m/z = 1767.96), and an N-terminal sequence, H_2N-^{1}MITIKK, as determined by Edman degradation. These results indicate that fragment A is the N-terminal region Met-1–Glu-106 (11.5 kDa) of the subunit (Fig. 4*C*). The partial digestion also produced an ~8-kDa fragment B with weak fluorescence that was identified as the peptide Val-94–Arg-172 (8.6 kDa) by Edman degradation (N-terminal sequence, H_2N-^{94}VAGDD) and MALDI-TOF MS (fragment, Thr-120–Arg-132, m/z = 1507.80, see Fig. 4*C*).

Next, the NqrA subunit labeled with PUQ-3 was cleaved using CNBr, producing a major fluorescent band whose apparent molecular mass was ~4 kDa (fragment D, Fig. 4*B*). Unfortunately, we were unable to identify fragment D by Edman degradation because multiple peptides from the CNBr digestion were contained in this region. However, considering the result of the V8 digestion and the theoretical cleavage sites for CNBr in the sequence, fragment D should be the peptide Ile-2–Met-39 (3.9 kDa), which contains a major binding site for PUQ-3 (Fig. 4*C*).

Another weakly fluorescent band from the CNBr digests of NqrA (fragment C) was assigned as His-44–Met-154 (12.1 kDa) by MALDI-TOF MS analysis of the tryptic digests (Phe-

[3] T. Ito, M. Murai, and H. Miyoshi, unpublished data.

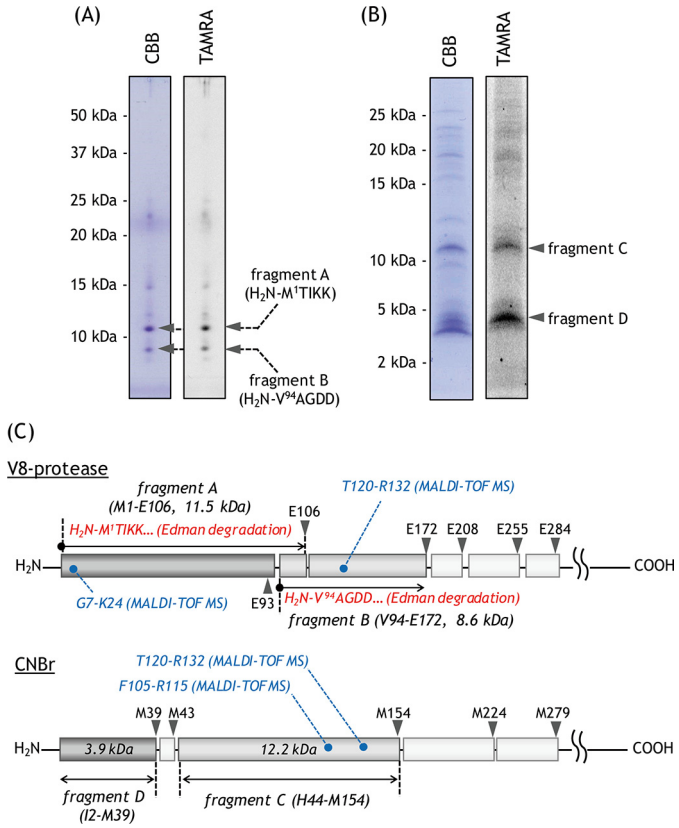

Figure 4. Localization of the region labeled by PUQ-3 in the NqrA subunit. *A,* partial V8-protease digestion of the NqrA subunit labeled by PUQ-3. Na^+-NQR (0.9 μM, 1.0 ml, 200 μg of protein) was labeled by PUQ-3 (10 μM), conjugated with TAMRA-N_3 via Cu^+-catalyzed click chemistry, followed by the separation on a 15% Laemmli-type SDS gel containing 6.0 M urea. The CBB-stained gel fragment containing the NqrA subunit (~5 μg of protein) was further subjected to in-gel partial digestion with V8-protease, followed by the separation on a 15% Tris-EDTA mapping gel. The N-terminal sequences of the CBB spots corresponding to the fluorescent spots were determined by Edman degradation. *B,* CNBr cleavage of the NqrA subunit labeled by PUQ-3. The NqrA labeled by PUQ-3 was conjugated with TAMRA-N_3 and cleaved with CNBr in 70% formic acid. The digests, which are equivalent to 10 μg of protein, were resolved by Schägger-type SDS gel (16% T, 6% C, containing 6 M urea). *C,* schematic presentation of the digestion of the NqrA subunit. The predicted cleavage sites are denoted by *arrows* and marked with their residue numbers in the sequences of the *V. cholerae* NqrA subunit (SwissProt entry Q9KPS1).

105–Arg-115 and Thr-120–Arg-132, m/z = 1262.68 and 1507.80, respectively). Fragment C shares sequence with fragment B (above) (Fig. 4*B*). Therefore, the region Val-94–Met-154, where fragments B and C overlap, may contain a minor binding site of PUQ-3. These two regions, which are likely to be involved in PUQ-3 binding, are highlighted in the structure in Fig. 1*B*; Ile-2–Met-39 is shown in *light* and *dark blue,* and Val-94–Met-154 is shown in *light* and *dark red*, respectively. In the crystallographic model, these two segments of NqrA are in close contact, but it must be remembered that this may not reflect the actual structure present throughout the catalytic cycle. Also, as discussed later, the fact that two regions are labeled by PUQ-3 does not necessarily indicate the presence of two distinct binding sites.

Photoaffinity labeling of Na^+-NQR by [^{125}I]PAD-2

A sample of Na^+-NQR (0.9 μM), which was washed with a buffer containing LDAO, was incubated with [^{125}I]PAD-2 (10 nM) in the presence of NADH and/or Q_1, irradiated with a UV lamp on ice, resolved on a 15% Laemmli-type SDS gel, and subjected to direct autoradiography. Because the detection sensitivity with ^{125}I labeling is quite high, we set the concentration of [^{125}I]PAD-2 as low as possible to reduce the probability of non-specific labeling. The radioactivity was exclusively incorporated into an ~30-kDa band, which corresponds to the NqrB subunit (Fig. 5*A*). The amount of radioactivity incorporated was ~50% lower in the presence of 100 μM NADH (Fig. 5*A*), but not in the presence of Q_1, suggesting that reduction of the cofactors may induce a structural change of the NqrB subunit.

The labeling of Na^+-NQR (0.9 μM) by [^{125}I]PAD-2 (10 nM) was repeated in the presence of other inhibitors as follows: aurachin D-42, korormicin, or PAD-2 (20 μM, 2000 mole excess over [^{125}I]PAD-2 in each case). Surprisingly, in the presence of each competitor, the amount of radioactivity incorporated into the NqrB subunit was significantly increased (Fig. 5*B*). It is important to note that this enhancement was observed in the presence of PAD-2, whose physicochemical properties are completely identical to those of [^{125}I]PAD-2, except for the radioactivity. To exclude the possibility that the enhancement of labeling is merely due to some structural alteration of the enzyme brought about by the high concentrations of hydrophobic chemicals, we conducted the same experiment in the presence of 20 μM bullatacin or antimycin A, which are potent and hydrophobic inhibitors of mitochondrial respiratory complexes I and III, respectively. Bullatacin and antimycin A did not affect the labeling yield of the NqrB subunit at all (data not shown). Thus, the enhancement of labeling must be due to specific binding of the competitors to Na^+-NQR.

We next changed the concentrations of aurachin D-42 and PAD-2, fixing the concentrations of Na^+-NQR (0.9 μM) and [^{125}I]PAD-2 (10 nM). The extent of the enhancement of labeling increased as the concentration of the competitors increased but then decreased slightly (Fig. 5*C*). We did not use concentrations of competitors over 50 μM because high concentrations of hydrophobic chemicals can disturb the enzyme structure in a non-specific manner.

To gain further insight into this seemingly peculiar phenomenon, we changed the molar ratio of Na^+-NQR to [^{125}I]PAD-2 (or competitor) by lowering the concentration of Na^+-NQR from 900 to 0.9 nM, while maintaining the concentrations of [^{125}I]PAD-2 and aurachin D-42 at 10 nM and 10 μM, respectively. Interestingly, the extent of enhancement of labeling brought about by aurachin D-42 decreased with a decrease in the concentrations of Na^+-NQR (Fig. 5*D*). The suppressive effect on the labeling became clearer at low concentrations of Na^+-NQR (0.9 and 9.0 nM). These results strongly suggest that the molar ratio of Na^+-NQR to [^{125}I]PAD-2 (or Na^+-NQR to competitor) is a critical factor determining the total amount of labeled enzyme. These effects of competitors on the photoaffinity labeling will be discussed below in the context of a proposed kinetic model.

Photoaffinity labeling of Na^+-NQR by [^{125}I]PAD-1

We also carried out photoaffinity labeling of Na^+-NQR (0.9 μM) using [^{125}I]PAD-1 (2.6 nM). As in the case of labeling with

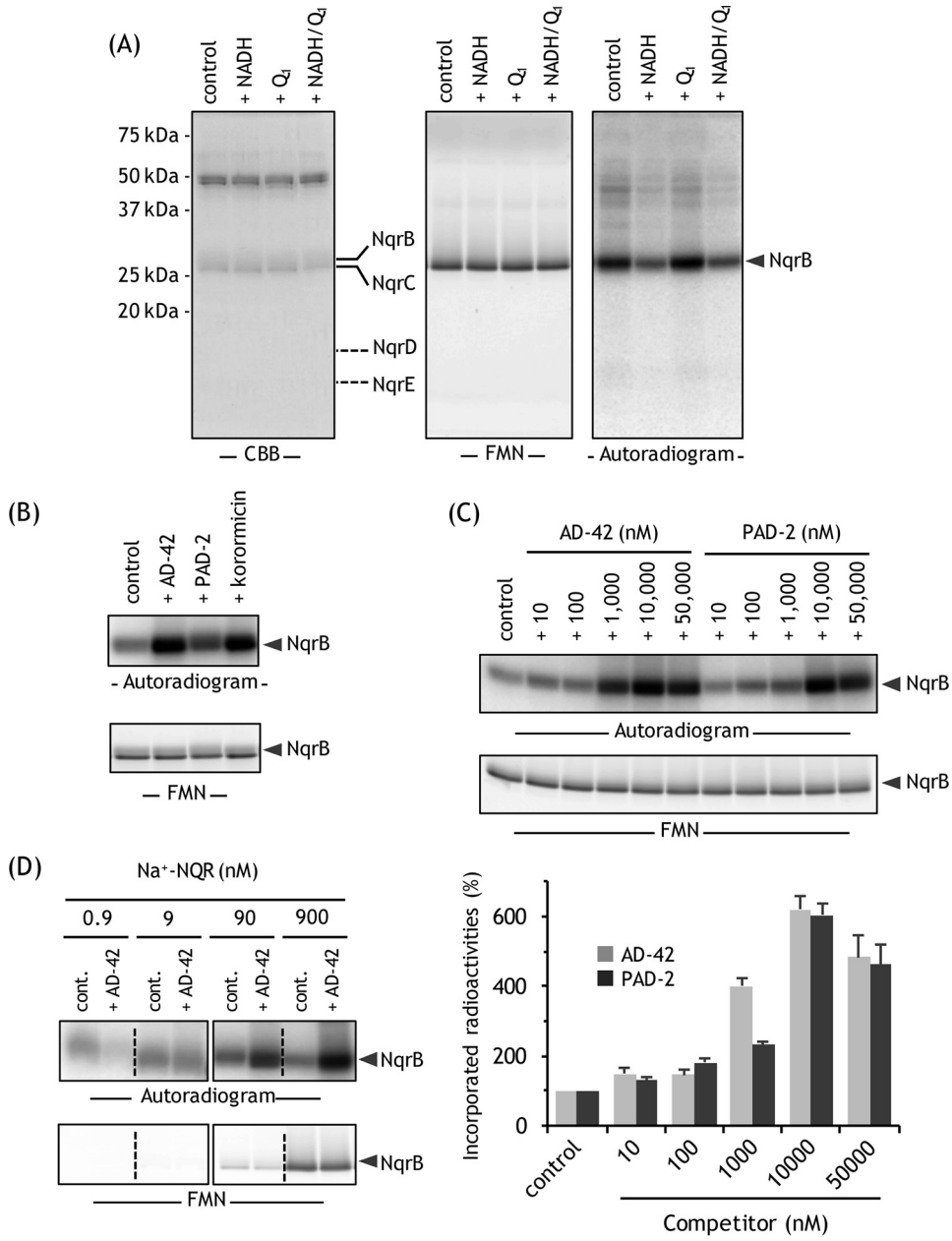

Figure 5. Photoaffinity labeling of Na^+-NQR by [^{125}I]PAD-2. *A,* Na^+-NQR (0.9 μM), washed with a buffer containing 0.05% LDAO, was incubated with [^{125}I]PAD-2 (10 nM) in the presence of NADH (100 μM) and/or Q_1 (50 μM). Then, the samples were photoirradiated with a UV lamp, resolved by a 15% Laemmli-type SDS gel, and subjected to CBB stain, fluorescent gel imaging (for bound-FMN), and autoradiography. Approximately 3 μg of proteins were loaded onto each well. *B,* effects of Na^+-NQR inhibitors on the specific labeling of the NqrB subunit. Na^+-NQR (0.9 μM) was labeled by [^{125}I]PAD-2 (10 nM) in the presence of an excess of aurachin D-42, PAD-2, or korormicin (20 μM each). The samples were analyzed according to the same procedures described above. *C,* effects of changing the concentrations of competitors on the labeling of the NqrB subunit. Na^+-NQR (0.9 μM) was labeled by [^{125}I]PAD-2 (10 nM) in the presence of increasing concentrations of aurachin D-42 or PAD-2 (10–50,000 nM), followed by SDS-PAGE and direct autoradiography. The yields of incorporated radioactivity are normalized by the band intensity in the absence of competitor (*control*). *D,* effects of changing the concentrations of enzyme on the labeling of the NqrB subunit. Na^+-NQR was labeled with [^{125}I]PAD-2 (10 nM) in the presence or absence of aurachin D-42 (10 μM) using different concentrations of the enzyme (0.9–900 nM). All data are representative of three independent experiments.

[^{125}I]PAD-2 (above), the radioactivity was exclusively incorporated into the NqrB subunit (Fig. 6*A*), and the yield was slightly lower in the presence of 100 μM NADH. It is important to note that although the inhibitory potency of [^{125}I]PAD-1, in terms of IC_{50} (0.9 nM Na^+-NQR), is much weaker than that of [^{125}I]PAD-2, the effectiveness of the labeling by [^{125}I]PAD-1 was comparable with that of [^{125}I]PAD-2. This was due to a much higher concentration of the enzyme (0.9 μM) used for the photoaffinity labeling experiment. To examine whether the unusual effect of competitors is also seen with [^{125}I]PAD-1, the photoaffinity labeling was repeated in the presence of an excess of aurachin D-42, korormicin, or PAD-1 (10 μM each, 4000 molefold of [^{125}I]PAD-1). In contrast to the case of [^{125}I]PAD-2, there was no clear enhancement of the labeling; but no significant competitive suppression was observed (Fig. 6*B*). It is noteworthy that the suppressive effect of aurachin D-42 became clearer at low concentrations of Na^+-NQR (Fig. 6*C*). Viewed in this light, the unusual effect of competitors on the pho-

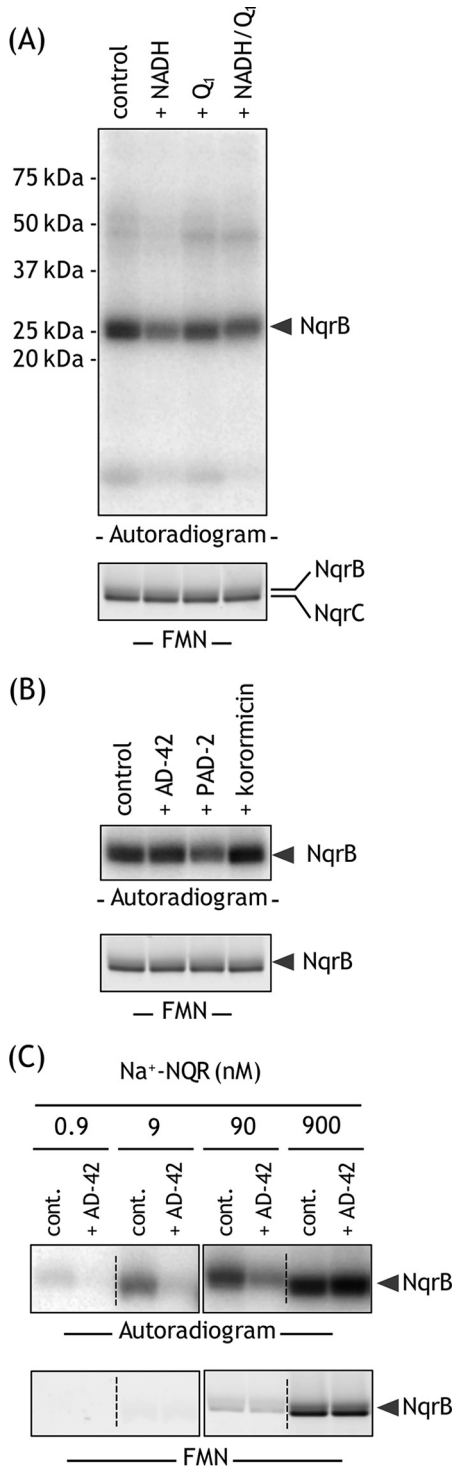

Figure 6. Photoaffinity labeling of Na^+-NQR by [^{125}I]PAD-1. *A*, Na^+-NQR (0.9 μM), washed with a buffer containing 0.05% LDAO, was incubated with [^{125}I]PAD-1 (2.6 nM) in the presence of NADH (100 μM) and/or Q_1 (50 μM). Then, the samples were photoirradiated with a UV lamp, resolved by a 15% Laemmli-type SDS gel, and subjected to CBB stain, fluorescent gel imaging (for bound-FMN), and autoradiography. Approximately 3 μg of protein was loaded onto each lane. *B*, effects of Na^+-NQR inhibitors on the specific labeling of the NqrB subunit. Na^+-NQR (0.9 μM) was labeled with [^{125}I]PAD-1 (2.6 nM) in the presence of an excess of aurachin D-42, PAD-1, or korormicin (10 μM each). The samples were analyzed according to the same procedures described above. *C*, effects of changing the concentrations of enzyme on the labeling of the NqrB subunit. Na^+-NQR was labeled by [^{125}I]PAD-1 (2.6 nM) in the presence or absence of aurachin D-42 (10 μM) using a range of different concentrations of the enzyme (0.9–900 nM). All data are representative of three independent experiments.

toaffinity labeling is a phenomenon common to [^{125}I]PAD-1 and [^{125}I]PAD-2, whereas the extent of the competitive suppression and the enhancement of the labeling differ between the two inhibitors because of their different chemical structures.

Localization of the site labeled by [^{125}I]PAD-1 and [^{125}I]PAD-2

To localize the region where [^{125}I]PAD-1 and [^{125}I]PAD-2 bind, the labeled NqrB subunit was isolated by SDS-PAGE and electroelution, followed by digestion with lysyl-endopeptidase (Lys-C) or endoprotease Asp-N. The Lys-C digestion of the NqrB subunit labeled by [^{125}I]PAD-2 (10 nM) gave the radioactive bands at ~8 (L1), ~7 (L3), and ~3 kDa (L4), whereas fluorescent gel imaging gave a single band due to bound FMN at ~18 kDa, which can be assigned to Glu-192–Lys-357 (17.9 kDa) (Fig. 7*A*). Considering that the fragment containing FMN (~18-kDa band) does not include the site labeled by [^{125}I]PAD-2, it is reasonable to consider that the radioactive bands at ~8 (L1), ~7 (L3), and ~3 kDa (L4) correspond to the regions Arg-43–Lys-121 (8.7 kDa), Arg-55–Lys-121 (7.3 kDa), and Trp-23–Lys-54 (3.7 kDa), respectively. The assignment to Arg-55–Lys-121 (7.3 kDa) was confirmed by N-terminal sequence analysis (H_2N-^{55}RIMIM) of the corresponding region on a CBB-stained PVDF membrane. These results show that [^{125}I]PAD-2 labels the two regions Arg-55–Lys-121 (L3) and Trp-23–Lys-54 (L4).

The Lys-C digests of the NqrB labeled by [^{125}I]PAD-1 (2.6 nM) gave radioactive bands at ~8 (L1′) and ~5 kDa (L2). Because the ~8-kDa fragment (L1′) is identical with that labeled by [^{125}I]PAD-2, the radioactive ~8-kDa (L1′) and ~5-kDa (L2) bands may be the regions Arg-43–Lys-121 (8.7 kDa) and Phe-6–Lys-54 (5.7 kDa), respectively, that share sequence Arg-43–Lys-54.

The Asp-N digestion of NqrB labeled by [^{125}I]PAD-1 or [^{125}I]PAD-2 afforded the same radioactive band with a molecular mass of ~9 kDa (A1) (Fig. 7*A*), which contains no FMN. Along with the results from the Lys-C digestion, this indicates that the ~9-kDa bands may be region Asp-9–Gly-89 (9.2 kDa). Thus, [^{125}I]PAD-1 and [^{125}I]PAD-2 label the N-terminal regions Arg-43–Lys-54 and Trp-23–Gly-89 (Fig. 7*B*), respectively, a part of the structure that protrudes from the membrane and forms a long stretch that anchors NqrA to the trans-membrane subunits (Fig. 1*C*). We cannot rule out the possibility that [^{125}I]PAD-2 labels two (or more) positions in the region Trp-23–Gly-89 because the side chain moiety of aurachin flexibly binds to the enzyme.

Inhibitor sensitivities of mutated Na^+-NQR

Hayashi *et al.* (15) discovered that a spontaneous mutation in the NqrB subunit of *Vibrio alginolyticus* Na^+-NQR, replacing Gly-140 with Val (corresponding to NqrB-Gly-141 in *V. cholerae* Na^+-NQR), confers a remarkable resistance against korormicin compared with the wild-type enzyme (approximately 5 orders of magnitude). In subsequent studies (8, 10), working with the *V. cholerae* Na^+-NQR, Barquera and co-workers demonstrated important functional roles for NqrB-Gly-140 and -Gly-141 in the electron transfer to ubiquinone. However, the effects of mutations at these positions on the inhibition of Na^+-

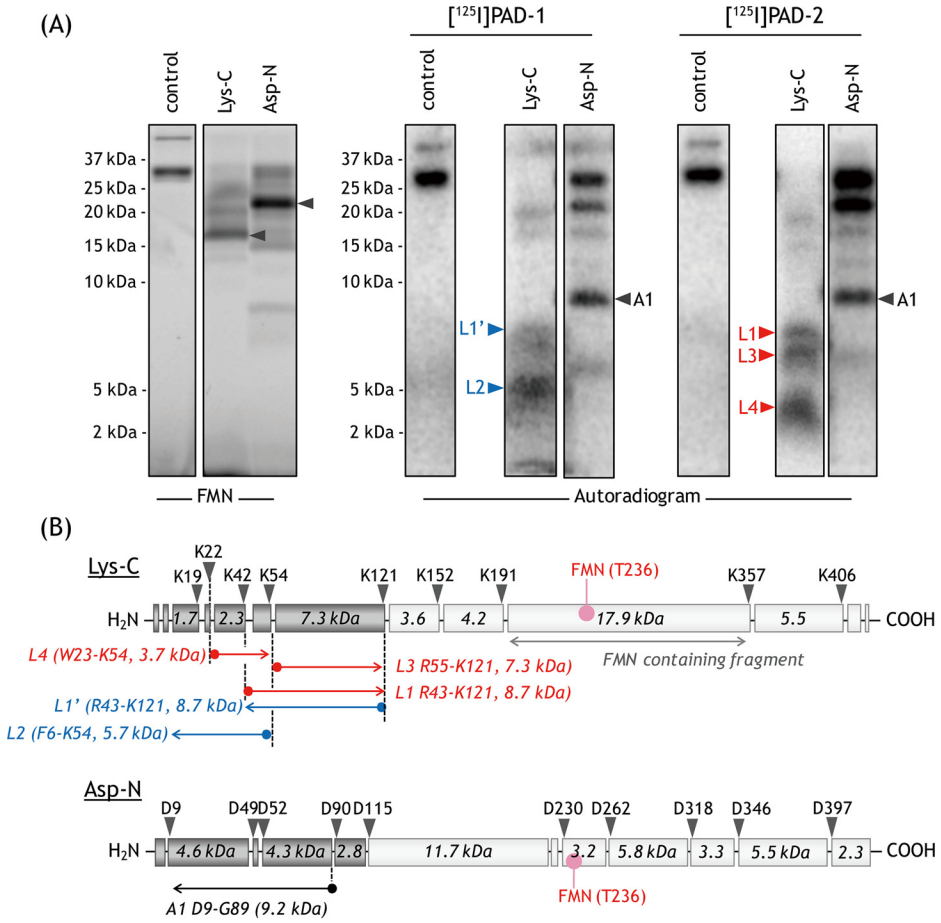

Figure 7. Localization of the region labeled by [^{125}I]PAD-1 and [^{125}I]PAD-2 in Na^+-NQR. *A*, Na^+-NQR (0.9 μM), labeled with [^{125}I]PAD-1 or [^{125}I]PAD-2 (10 nM), was separated on a 16% Shägger-type SDS gel (16% C, 3% T), followed by the partial isolation of the NqrB subunit by electroelution. The labeled NqrB subunit was digested with Lys-C or Asp-N, and the digests were resolved by SDS-PAGE using a 16% Shägger-type SDS gel (16% C, 6% T containing 6 M urea). The SDS gel was subjected to fluorescent gel imaging (for bound FMN) and autoradiography. *B*, schematic presentation of the digestion of the NqrB subunit by Lys-C or Asp-N. In the digestion map for Lys-C, the fragments derived from NqrB labeled by [^{125}I]PAD-1 and [^{125}I]PAD-2 are indicated by *blue* and *red arrows*, respectively. FMN phosphorylthreonine (Thr-236 (22, 23)) is marked by a *pink circle*. The predicted cleavage sites are denoted by *arrows* and marked with their residue numbers in the sequences of *V. cholerae* NqrB subunit (SwissProt entry Q9KPS2).

NQR by korormicin were not studied at that time because the inhibitor was not available.

We have now examined changes in the inhibitor sensitivity of five mutant enzymes, three with substitutions in helix II of NqrB, near the spontaneous mutation identified by Hayashi *et al.* (15) (G140A, G141V, and E144C in the NqrB subunit), and two at the rear wall of the putative ubiquinone-binding cavity (Y36A and G38V in the NqrA subunit), as described above, using korormicin, aurachin D-42, PAD-1, PAD-2, and HQNO (Table 1). The inhibitor sensitivity, in terms of IC_{50} value, of NqrA-Y36A and -G38V were essentially unchanged compared with the wild-type enzyme. In contrast, NqrB-G140A and -E144C exhibited remarkable resistance against all inhibitors tested (at least 1000-fold); the inhibitors lost their effectiveness almost completely. For NqrB-G141V, the inhibitor sensitivities to aurachin D-42, PAD-2, and HQNO were very similar to those of the wild-type enzyme, whereas the sensitivities to PAD-1 and korormicin were reduced by a factor of ~10 and ~100, respectively. These results indicate that NqrB-Gly-140 and -Glu-144, in transmembrane helix II of NqrB, are critical for the interference of the enzyme function by these inhibitors, whereas Gly-141 appears to play a lesser role.

Photoaffinity labeling of Na^+-NQR mutants by [^{125}I]PAD-2

The remarkable resistance of the NqrB-G140A and -E144C mutants against the inhibitors would typically indicate that the inhibitors are no longer able to bind to the mutated enzymes. To check this, we carried out the photoaffinity labeling on the mutants using [^{125}I]PAD-2. Unexpectedly, the labeling yields did not decrease compared with the wild-type enzyme, but rather they remained the same or, in the case of NqrB-G140A, increased (Fig. 8*A*). The fact that the mutated enzymes were labeled in apparently the same manner as the wild-type enzyme indicates that the sites that bind the inhibitors in the wild type have not been destroyed by the mutations, although the inhibitory effect has disappeared. It is noteworthy that the presence of aurachin D-42 or korormicin significantly enhanced the labeling of NqrB-E144C by [^{125}I]PAD-2 (Fig. 8*B*), as observed for the wild-type enzyme (Fig. 5*B*). For the G140A mutant, labeling was not affected by the presence of aurachin D-42 or korormicin. The labeling yields with the NqrA-Y36A and

Table 1

The inhibitory activities of different inhibitors with the wild type and mutated Na^+-NQR

The inhibitory activity, in terms of the IC_{50} value (nM), was examined with the NADH-Q_1 oxidoreductase activity using isolated Na^+-NQR (0.9 nM). When 50% inhibition was not observed, the residual enzyme activities (%) at the indicated concentrations are shown in parentheses. Data shown are mean values ± S.D. (n = 3–4).

	HQNO	Korormicin	Aurachin D-42	PAD-1	PAD-2
WT	2000 (±250)	5.0 (±0.70)	2.0 (±0.30)	590 (±45)	1.6 (±0.21)
NqrA-Y36A	3100 (±330)	8.1 (±0.87)	2.7 (±0.22)	830 (±70)	3.3 (±0.41)
NqrA-G38V	4500 (±360)	8.0 (±0.91)	2.8 (±0.28)	960 (±87)	5.7 (±0.50)
NqrB-G140A	>200,000 (~95%)	>50,000 (~90%)	>12,000 (~80%)	>27,000 (~100%)	>10,000 (~100%)
NqrB-G141A	1200 (±170)	820 (±77)	3.3 (±0.14)	5200 (±610)	1.3 (±0.11)
NqrB-E144C	>200,000 (~60%)	>50,000 (~70%)	>12,000 (~60%)	>27,000 (~100%)	>10,000 (~80%)

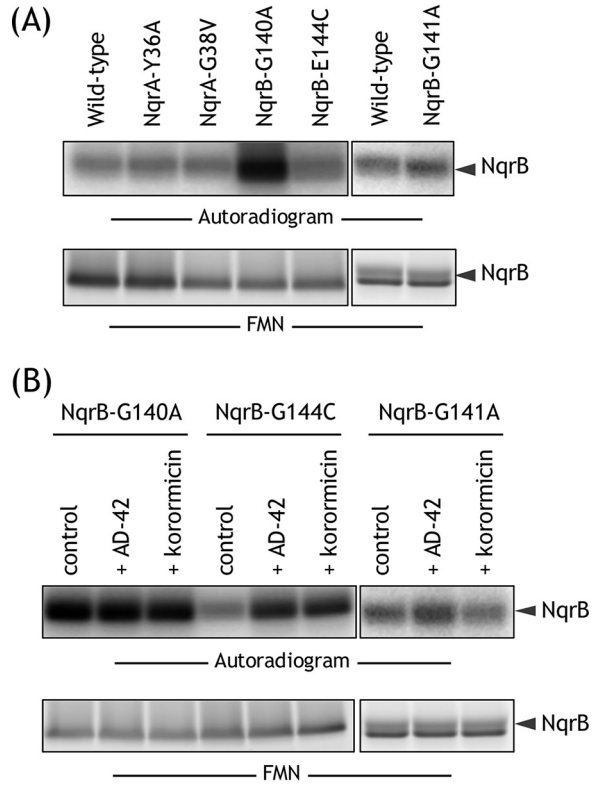

Figure 8. Photoaffinity labeling of the Na^+-NQR mutants by [^{125}I]PAD-2. *A*, LDAO-washed mutant Na^+-NQRs (Y36A and G38V in NqrA and G140A, G141A, and E144C in NqrB) were labeled with [^{125}I]PAD-2 (10 nM) at a protein concentration of 0.9 μM. The samples were resolved on a 15% Laemmli-type SDS gel and subjected to fluorescent gel imaging or autoradiography. *B*, NqrB mutants were also labeled in the presence of an excess of aurachin D-42 or korormicin (10 μM each). The autoradiogram of the control lane of the NqrB-G141A in *B* is the same as that used in the NqrB-G141A lane in *A*. All data are representative of three independent experiments.

-G38V mutants were unchanged compared with the wild-type enzyme (Fig. 8*A*).

Discussion

Na^+-NQR from *V. cholerae* has been extensively investigated using a wide variety of techniques; however, the positions of the binding sites for ubiquinone and inhibitors in this enzyme remain controversial. Steuber *et al.* (13) identified a deep solvent-accessible cavity, in the NqrA subunit, in their crystallographic structure, and pointed out that it could accommodate a ubiquinone molecule. Now, to more precisely locate the binding sites for ubiquinone and inhibitors, we have carried out photoaffinity labeling experiments with a photoreactive ubiquinone (PUQ-3) and two different aurachin-type inhibitors ([^{125}I]PAD-1 and [^{125}I]PAD-2) using the isolated Na^+-NQR.

The photoaffinity labeling experiment using PUQ-3 showed that the ubiquinone ring binds primarily in the region Ile-2–Met-39 of NqrA and secondarily in the region Val-94–Met-154 of the same subunit (Fig. 4). We were unable to pinpoint the labeled residue(s) exactly because of low labeling yield. Nevertheless, some parts of these regions can be ruled out as candidates for the binding site of the ubiquinone ring because they lie on the exterior surface of NqrA, on the opposite side of the subunit from the likely position of the riboflavin cofactor in NqrB, and thus too far away for efficient electron transfer; these include the sequence stretches Ile-2–Leu-31 and Val-94–Phe-130, thus leaving Leu-32–Met-39 and Phe-131–Met-154 as the remaining candidates. The fact that there is labeling in two different stretches of the sequence does not necessarily require the existence of two different binding sites for ubiquinone. In the crystallographic structure, the folding of NqrA brings the two labeled stretches together, and ubiquinone could adopt two slightly different bound conformations at the same locus; the rod-like azido ($-N=N^+=N^-$) group would then cross-link in different places reflecting the two conformations. The two labeled stretches come into closest contact in the region of Leu-32–Met-39 and Phe-131–Lys-138 of NqrA (*orange circle* in Fig. 1*B*), which together form a highly plausible binding location for the ubiquinone ring. It is important to note that, although these stretches of polypeptide form the rear wall of the putative ubiquinone-binding cavity in the crystallographic structure (13), the actual size, shape, and position of the cavity may not be the same at all times throughout enzyme turnover, as mentioned in the Introduction. The labeling by PUQ-3 was effectively suppressed by short-chain quinones (Q_2 and 3-N_3-Q_2) confirming the likely role of this location as the catalytic quinone reduction site. However, labeling was not suppressed by the potent inhibitors aurachin and korormicin (Fig. 3*B*), indicating that the binding position of ubiquinone does not overlap those of the inhibitors. A previous photoaffinity labeling study using a different photoreactive ubiquinone also showed that the ubiquinone ring binds to NqrA (7); however, in that case the labeled region was not further defined.

Photoaffinity labeling with [^{125}I]PAD-1 and [^{125}I]PAD-2 showed that the toxophoric quinolone ring of aurachin and its alkyl side chain both bind to NqrB, but in two different stretches of polypeptide (Arg-43–Lys-54 and Trp-23–Gly-89, respectively) within the N-terminal portion of the subunit. These two segments are part of a region that protrudes from the membrane and forms a long stretch that attaches to the NqrA subunit, anchoring it to the integral membrane subunits of the enzyme (Fig. 1*C*). Although the structure of the region Met-1–Pro-37 is not included in the model of Steuber *et al.* (13), this

N-terminal region would apparently form a part of the wall of the putative quinone-binding pocket identified above, because Gly-38 –Leu-53, which follows immediately in the sequence, lies in a groove neighboring the cavity in NqrA. Together, the results from the photoaffinity labeling with PUQ-3, [^{125}I]PAD-1, and [^{125}I]PAD-2 indicate that the binding positions of ubiquinone and aurachins do not overlap one another, even though aurachin-type inhibitors resemble the ubiquinone molecule in structure. It is thus likely that the inhibitors perturb the reaction of ubiquinone indirectly by binding to a site or sites in the N-terminal region of NqrB and causing a conformational change. This notion is consistent with the results obtained in earlier steady-state kinetic studies (11, 24, 25), which showed that HQNO and korormicin do not compete directly with ubiquinone.

It is generally thought that "quinone-analog" inhibitors of respiratory enzymes occupy the quinone-binding cavity in a manner competitive with quinone. However, this is not necessarily true of all respiratory inhibitors. For example, piericidin A is extremely similar to the ubiquinone molecule but is a highly selective inhibitor of mitochondrial complex I and has no effect on other enzymes, including those that interact with quinone/quinol. Moreover, there are a number of inhibitors that work by binding to the quinone-binding cavity of various enzymes but lack any strong structural resemblance to ubiquinone, for example antimycin A analogs, inhibitors of Qi site in complex III (26), and various inhibitors of Qo site in complex III (*e.g.* myxothiazol and famoxadone) (27). Thus, the modes of action of respiratory inhibitors cannot always be inferred from their structural similarity to ubiquinone.

The results obtained in this study raise two interesting questions. First, in light of the fact that PAD-1 and PAD-2 lose their inhibitory activities almost completely against the NqrB-G140A and -E144C mutants (Table 1), why does the effectiveness of labeling of [^{125}I]PAD-1 and [^{125}I]PAD-2 to the mutated enzymes not change compared with the wild-type enzyme (Fig. 8*A*)? Second, how is it that the effects of competitor molecules on photoaffinity labeling by [^{125}I]PAD-1 and [^{125}I]PAD-2 can change in opposite directions (suppression *versus* enhancement) depending on the concentrations of the enzyme and competitor (Figs. 5*D* and 6*C*)? It is obvious that these results are not consistent with a simple scenario in which the different inhibitors share a common binding pocket, and where NqrB-Gly-140 and -Glu-144 lie within this pocket and interact directly with the inhibitors. Instead, we must assume that there is a dynamic interaction between the adjacent subunits NqrA and NqrB, which regulates the reaction of ubiquinone and inhibitors with the enzyme. In this scenario, NqrB-Gly-140 and -Glu-144 would play key roles in the interaction of the two subunits.

To address the first question, we will present models for the catalytic reaction of the wild-type Na^+-NQR (Fig. 9*A*) and the mutants (Fig. 9*B*) in the presence and absence of inhibitor. These models are based on the results of our previous kinetic study of Na^+-NQR showing that ubiquinone binds to Na^+-NQR only after the enzyme becomes reduced by accepting electrons from NADH (11). In addition, we will adopt the working hypothesis that a large conformational change in the NqrB subunit takes place during enzyme turnover, shortening the distance between the ubiquinone-binding pocket in NqrA and the riboflavin in NqrB, thus facilitating efficient electron transfer (supposition i). Because the existence of a high-affinity bound quinone in isolated Na^+-NQR (in substoichiometric amounts) and its catalytic role have not yet been definitively established, we will not discriminate between bound and catalytic quinones in this model.

To assess validity of supposition i, we again consider the structural information obtained from the crystallographic study of *V. cholerae* Na^+-NQR (13). The distances between several pairs of redox centers in the proposed electron transfer pathway are too long for physiologically relevant electron transfer: for example, between the [2Fe-2S] in NqrF and the iron in NqrD-E and between the FMN in NqrB and the riboflavin in NqrB. Facile electron transfer between these redox centers cannot be explained without the assumption that large conformational changes take place during enzyme turnover and that these changes have the effect of decreasing each one of these electron transfer distances at some point during the catalytic cycle (13). The same is true for the distance between the "crystallographic" positions of the putative ubiquinone-binding cavity in NqrA and the riboflavin in NqrB.

According to our model, the catalytic cycle of wild-type enzyme would proceed as shown in Fig. 9*A*. Although the ubiquinone-binding pocket is initially located far from the riboflavin in the oxidized form of Na^+-NQR, a conformational change in the NqrB subunit (or at the interface between NqrA and NqrB), triggered by reduction of one or more cofactors, including the riboflavin in NqrB, causes the spatial gap between the riboflavin and the ubiquinone ring to decrease, thus facilitating efficient electron transfer. The upward movement of the NqrB subunit shown in Fig. 9*A* represents this conformational change. The bound inhibitor could serve as a "wedge" at the interface between NqrA and NqrB, which prevents the conformational change in NqrB required for efficient electron transfer.

Our model also accounts for the effects of mutations on the same steps in the catalytic cycle, as described above. Our earlier FTIR spectroelectrochemical study demonstrated that the NqrB-G140A mutation does not alter the midpoint potentials of any of the redox cofactors or the overall structure of the enzyme, compared with the wild type. The mutant enzyme has a much lower V_{max} for steady-state turnover, but the K_d value for quinone is not significantly changed from wild type. Consistent with this, mutation markedly decreases the rates of both the forward electron transfer from the riboflavin cofactor to ubiquinol (10) and reverse reaction (8). Taken together, these results suggest that a change in the size of the residue at position 140 in the NqrB sequence has an indirect effect on the reaction of ubiquinone in some way but also that this residue is not part of the domain that makes up the actual binding site for ubiquinone. This is illustrated in Fig. 9*B*, where the distance between the riboflavin and the quinone site has been slightly increased relative to the wild-type enzyme (Fig. 9*A*) to reflect a perturbed but still functioning electron transfer step between the two sites (10). It is worth noting that the same FTIR spectroelectrochemical study also found evidence for structural differences in the environment surrounding a bound inhibitor (HQNO)

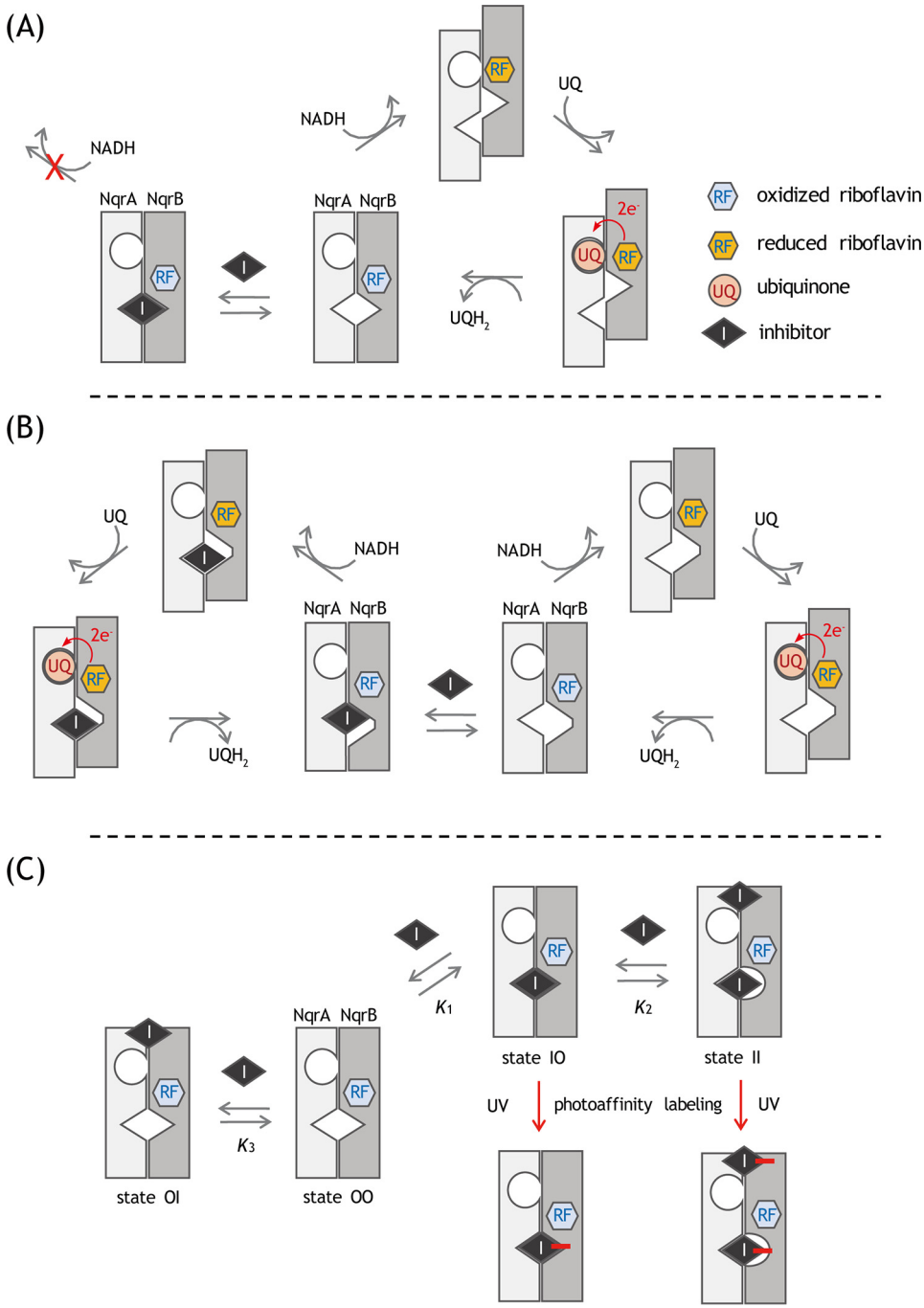

Figure 9. Models for the catalytic reaction of the wild-type Na^+-NQR (*A*) and the G140A mutant (*B*). The reduction of cofactors by NADH induces a conformational change of NqrB (indicated as an upward movement of the subunit), which decreases the gap between riboflavin and the ubiquinone-binding pocket, facilitating electron transfer. The bound inhibitor serves as a "wedge" and interferes with the conformational change of NqrB required for the electron transfer. The G140A mutant may be able to undergo the conformational change even in the presence of inhibitor because of structural alteration of the environment surrounding the inhibitor. *C,* model of the photoaffinity labeling with the wild-type Na^+-NQR in the presence of competitor. The model postulates two inhibitor-binding sites in Na^+-NQR to give three inhibitor-bound states (states "OI," "IO," and "II"), which are defined by three association constants K_1, K_2, and K_3. We assume that K_3 is negligibly small compared with K_1 and K_2 and, crucially, that the sum of the yields of labeling reaction at the both sites in state II is considerably higher than the yield in state IO.

between the wild-type enzyme and the mutants (NqrB-G140A and -G141V) (10). Thus, it appears likely that in the mutants the structural rearrangement of NqrB, due to the reduction of cofactors, may be able to take place even in the presence of bound inhibitor. This is illustrated in our scheme (Fig. 9, *A* and *B*); in the wild-type enzyme, the inhibitor serves as a wedge to block the normal conformational change (shown as upward shift of NqrB), preventing a decrease in the distance between the riboflavin cofactor and ubiquinone and thus impeding fast electron transfer (Fig. 9*A*). In the mutants, a structural alteration of the pocket surrounding the inhibitor creates sufficient additional space or flexibility that the inhibitor is no longer able to prevent the conformation change, and thus facile electron transfer from riboflavin to ubiquinone takes place

(Fig. 9*B*). Thus, our scheme may answer the first question as to why aurachin derivatives maintain high binding affinities to the mutated enzymes (G140A, G141V, and E144C) without interfering with electron transfer from the riboflavin to ubiquinone.

Next, we consider the second question. Why does the effect of competitors on the photoaffinity labeling by [^{125}I]PAD-1 and [^{125}I]PAD-2 change in opposite directions (suppression *versus* enhancement) depending on the concentrations of the enzyme and competitor? It should be emphasized that the same effect on labeling was also observed using cold ligands (PAD-1 and PAD-2) and hot ligands ([^{125}I]PAD-1 and [^{125}I]PAD-2) together and also that the enhancing effect of competitors manifested itself at much higher inhibitor concentrations than those required for complete inhibition of the enzyme activity. We tried using a number of different kinetic models to simulate the total amount of labeled Na^+-NQR under different experimental conditions. However, it became clear that this phenomenon cannot be explained unless our model includes two distinct inhibitor-bound states in which the yields of the labeling reaction are considerably different. Furthermore, the equilibrium between the two inhibitor-bound states must be controlled by the inhibitor concentration, meaning that there needs to be two binding sites for the inhibitor that have different affinities. An example of such a model is shown in Fig. 9*C*, where there are two inhibitor-bound states (IO and II), and the yield of labeling in state II (the sum of the yields at the both sites) is considerably higher than in IO (supposition ii). It would not be surprising if the reactivity of the aryl azido ($-N=N^+=N^-$) groups in PAD-1 and PAD-2 (and their ^{125}I-labeled derivatives) changes with variations in the binding environment. In our scheme, the putative second molecule of inhibitor is provisionally shown at the interface of the NqrA and B subunits.

The scheme in Fig. 9*C* includes free inhibitor (I), free enzyme (state OO), and three inhibitor-enzyme complexes (states OI, IO, and II), which leads to the following equilibrium Equations 1–3,

$$K_1 = \frac{[IO]}{[OO][I]} \quad \text{(Eq. 1)}$$

$$K_2 = \frac{[II]}{[IO][I]} \quad \text{(Eq. 2)}$$

and

$$K_3 = \frac{[OI]}{[OO][I]} \quad \text{(Eq. 3)}$$

Mass conservation conditions for the inhibitor and enzyme gives Equations 4 and 5,

$$[OO] + [IO] + [II] + [OI] = [E]_0 \quad \text{(Eq. 4)}$$

and

$$[IO] + 2[II] + [OI] + [I] = [I]_0 \quad \text{(Eq. 5)}$$

where $[I]_0$ and $[E]_0$ are the total concentrations of the inhibitor and the enzyme, respectively. Assuming that the yields of the labeling reactions are 10% for the IO state and 90% for the II state (sum of the yields at the two binding sites because in this state both are occupied), the total amount of Na^+-NQR labeled by [^{125}I]PAD-2 and PAD-2 (which are chemically identical) is given by {0.1[IO] + 0.9[II]}; in other words, the incorporated radioactivity is proportional to Equation 6,

$$\{0.1[OI] + 0.9[II]\} \quad \text{(Eq. 6)}$$

Equations 1–6 could then be numerically solved using Mathematica® (Wolfram). For this analysis, we further assume that the inhibitor does not bind to the second site unless the first site is already occupied by a molecule of the inhibitor (*i.e.* state OI scarcely exists: $K_1, K_2, \gg K_3$), as discussed below. Thus, for the current simulation we set K_1, K_2, and K_3 to 1000, 800, and 1 mM^{-1}, respectively. Based on these assumptions, the total amount of Na^+-NQR labeled by [^{125}I]PAD-2 and PAD-2 is a sigmoid function of the total inhibitor concentration. This relationship is shown for four different enzyme concentrations in Fig. 10*A*.

Fig. 10*B* shows the relative amount of radioactivity incorporated into Na^+-NQR by [^{125}I]PAD-2 (10 nM) as a function of the concentration of added PAD-2, normalized so that the value at zero-added PAD-2 is one, as calculated from the data in Fig. 10*A*. Values below one indicate competitive suppression of labeling, whereas values above one indicate enhancement. It should be noted that our model (Fig. 9*C*) can account for the *consecutive* changes of the effects of competitor (from suppression to enhancement and back to suppression) as the concentration of the competitor increases relative to that of the enzyme. Considering that the extent of suppressive or enhancing effects vary depending on the parameters (K_1, K_2, and the reaction yields in the states IO and II) that are determined by the individual chemical structures of the inhibitor, the small difference in the effects of competitors between [^{125}I]PAD-1 and [^{125}I]PAD-2 can easily be accounted for (Figs. 5 *versus* 6).

To determine the binding site for the second molecule of inhibitor, we examined the Lys-C digestion pattern of the NqrB subunit labeled by [^{125}I]PAD-2 (10 nM) in the presence of aurachin D-42 (10 μM). As shown in Fig. 11, the resulting digestion pattern was almost identical to that observed in the absence of aurachin D-42, but the labeling intensity at the ~8-kDa band (Arg-55–Lys-121) relative to other bands was significantly higher, suggesting that a second molecule of the inhibitor binds to this region. The structure around this region may change in the presence of the first molecule of inhibitor to allow the binding of the second molecule of inhibitor. The binding of the second molecule may, in turn, affect the bound state of the first molecule of inhibitor, resulting in an increase in the reaction yield in state II.

Although we cannot rule out other scenarios that might explain these apparently paradoxical results, our model gives a possible explanation for them. The model is also able to explain the effects of competitor molecules on the photoaffinity labeling of the mutants. The labeling yield for NqrB-G140A mutant was significantly higher even in the absence of a competitor compared with the wild-type, G141V, and E144C mutants (Fig.

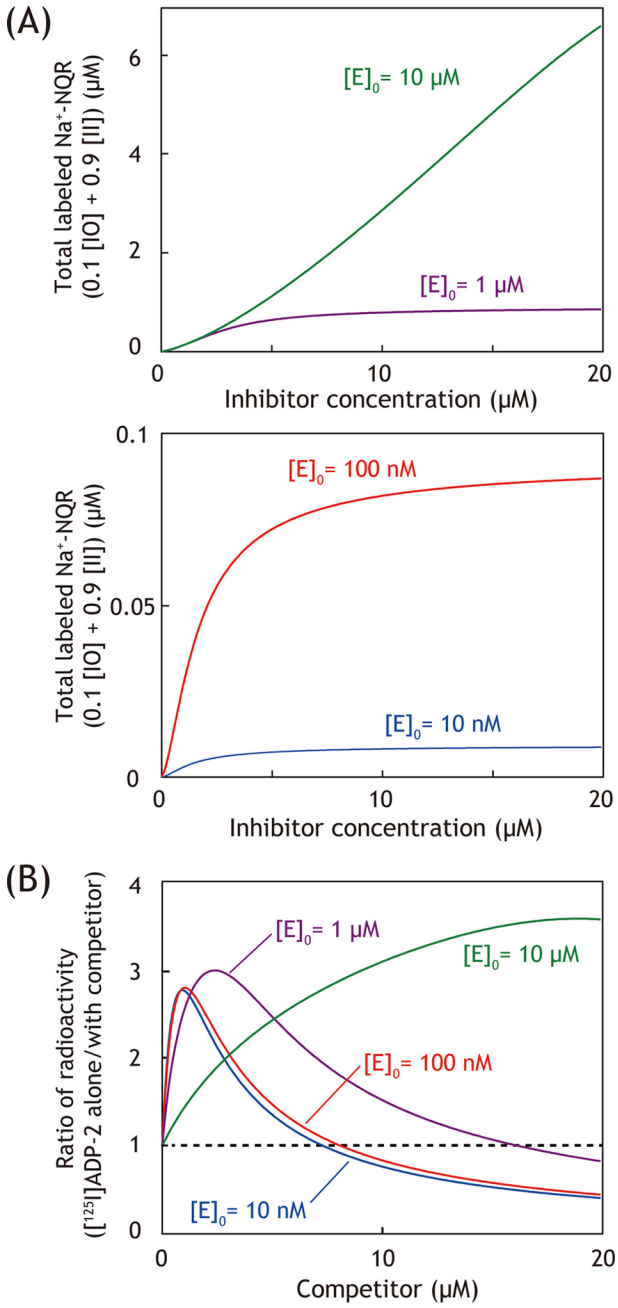

Figure 10. *A,* simulation of a total amount of the labeled Na^+-NQR. The total amount of Na^+-NQR labeled by [^{125}I]PAD-2 and PAD-2 is defined as {0.1[IO] + 0.9[II]} according to the simulation described under the "Discussion." The concentrations of total enzyme ($[E]_0$) are indicated in the figure. *B,* ratio of the incorporated radioactivity in the absence of PAD-2 (10 nM [^{125}I]PAD-2 alone) to that in the presence of PAD-2 (competitor) changes with the concentrations of PAD-2. The ratio was estimated from the data shown in *A*.

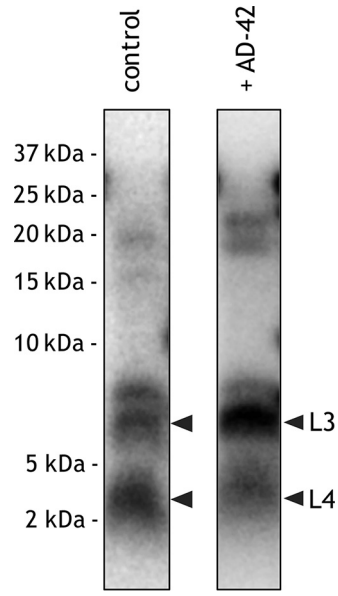

Figure 11. Photoaffinity labeling by [^{125}I]PAD-2 in the presence of an excess of aurachin D-42. Na^+-NQR (0.9 μM) was labeled with [^{125}I]PAD-2 (10 nM) in the presence of an excess of aurachin D-42 (10 μM). The labeled NqrB subunit was isolated and digested by Lys-C according to the same procedures as those described in the Fig. 7, followed by the SDS-PAGE using a 16% Schägger-type SDS gel (16% C, 6% T containing 6.0 M urea). The autoradiogram "control" is the same as that used in Fig. 7*A*.

8*A*) and was not enhanced in the presence of a competitor. This unique behavior of the NqrB-G140A mutant can also be reproduced in the model if we assume $K_1 \gg K_2$ (*e.g.* 1000:100). It should be remembered that the inhibitor sensitivities are considerably different between G141V and G140A (or E144C) (Table 1). Taken together, the mode of interaction between the ligands and Na^+-NQR may vary in a complicated way depending on the structural changes in the NqrB subunit (or interfacial regions between NqrB and NqrA) induced by the different mutations. Because of this complexity, it is difficult to provide a complete scenario at present, which can explain all the details of the results obtained in this study. Gly-140, Gly-141, and Glu-144 are located in a transmembrane helix II of the NqrB subunit and do not make a direct contact with other subunits (13). This study revealed that these residues do not participate directly in the binding sites of ubiquinone and inhibitor. As there is currently no information about structural changes brought about by these mutations, the roles of the residues in the regulation of structural changes of the NqrB subunit (or interfacial regions between NqrA and NqrB subunits) remain to be investigated.

In conclusion, this study demonstrates that the solvent-accessible cavity in the NqrA subunit, revealed by the recent X-ray crystallographic study and predicted to accommodate ubiquinone (13), does in fact include a site for ubiquinone binding. However, the position, size, and shape of this cavity in the crystallographic model may not be the ones maintained throughout actual enzyme turnover. Aurachin-type inhibitors (and presumably also korormicin) interfere indirectly with the electron transfer from the riboflavin cofactor to ubiquinone, presumably via blocking a conformational change involving the NqrB subunit by binding to the long N-terminal stretch of the subunit. The base part of this N-terminal stretch closest to the transmembrane helices of the subunit is able to accommodate the second molecule of inhibitor in high concentration conditions. NqrB-Gly-141, Gly-140, and Glu-144, located in transmembrane helix II, may confer resistance against aurachin (and korormicin), apparently by interfering with dynamic conformational changes in NqrB or at the interface between NqrA and NqrB.

Experimental procedures

Materials

Ubiquinone-1 (Q_1) was a kind gift from Eisai (Tokyo, Japan). 3-N_3-Q_2 was synthesized as described previously (28). Protein standards (Precision Plus Protein Standards) for SDS-PAGE were purchased from Bio-Rad. The Click-iT reaction buffer kit and TAMRA-azido (18–20) were purchased from Life Technologies, Inc. [^{125}I]NaI was purchased from PerkinElmer Life Sciences. DDM and LDAO were purchased from Dojin (Kumamoto, Japan) and Sigma. Other reagents were all of analytical grade.

Syntheses of PUQ-3, PAD-1, [^{125}I]PAD-1, PAD-2, and [^{125}I]PAD-2

The synthetic procedures for PUQ-3, PAD-1, and PAD-2 (including their ^{125}I-incorporated derivatives, [^{125}I]PAD-1 and [^{125}I]PAD-2) are described in the supplemental Schemes 1–5. All compounds were characterized by ^{1}H and ^{13}C NMR spectroscopy and mass spectrometry.

Isolation of korormicin

Korormicin was isolated from the marine bacterium *Pseudoalteromonas* strain J010 cells (a kind gift from Tillman Harder and Jan Tebben) according to the reported methods with some modifications (16, 17). Cells were grown in fermenters in 30-liter batches in marine broth (Difco) at 28 °C with constant agitation (300 rpm) and aeration (20 liters/min). Cells were harvested in late stationary phase (48 h), washed with 50 mM Tris-HCl, pH 8, 300 mM NaCl, and frozen at −80 °C until used.

The cell pellet of *Pseudoalteromonas* strain J010 (50 g) was extracted with ethanol for 2 h at room temperature; the extraction was repeated three times. The combined extracts were centrifuged at 2500 rpm for 10 min at 4 °C, and then the supernatant was collected and concentrated under reduced pressure to afford the extract residue (3.25 g). After the residue (1.56 g) was partitioned with diethyl ether (3 × 30 ml) and water (40 ml), the fraction extracted with diethyl ether was dried over anhydrous $MgSO_4$ and concentrated to afford the diethyl ether fraction (336 mg). The diethyl ether fraction was chromatographed on a silica gel column (15 × 120 mm, Wako Gel® C-200) and eluted with 5, 10, 30, 50, and 100% ethyl acetate/*n*-hexane. Only the fraction eluted with 50% ethyl acetate/*n*-hexane elicited the inhibition of the NADH-Q_1 oxidoreductase activity of Na^+-NQR. This 50% fraction (12 mg) was further purified by reversed phase HPLC (20 × 250 mm, COSMOSIL 5C_{18}-MS-II, 80% methanol, 0.1% formic acid, detected at 254 nm) with a flow rate of 5.0 ml/min at 30 °C to provide korormicin as a colorless oil (5.6 mg, 12 μmol, retention time is 54.2 min). The following spectral data completely corresponded to those reported previously (16, 17); $[\alpha]_D^{24}$ −23.6 (c = 0.28, EtOH); ^{1}H NMR (500 MHz, $CDCl_3$): δ 8.33 (s, 1H), 7.37 (s, 1H), 6.46 (ddd, J = 15.1, 11.3, 1.0 Hz, 1H), 6.09 (t, J = 11.1 Hz, 1H), 5.84 (dt, J = 15.1, 7.2 Hz, 1H), 5.40 (dd, J = 9.8, 9.0 Hz, 1H), 5.06 (td, J = 8.6, 2.7 Hz, 1H), 2.99 (ddd, J = 11.0, 8.0, 6.1 Hz, 1H), 2.98 (ddd, J = 10.9, 8.2, 6.1 Hz, 1H), 2.63 (dd, J = 15.8, 8.6 Hz, 1H), 2.57 (dd, J = 15.7, 3.4 Hz, 1H), 2.35 (t, J = 6.1 Hz, 2H), 1.99–1.76 (m, 2H), 1.56–1.51 (m, 2H), 1.49 (s, 3H), 1.48–1.27 (m, 12H), 0.90 (t, J = 7.5 Hz, 3H), 0.88 (t, J = 7.5 Hz, 3H); ^{13}C NMR (125 MHz, $CDCl_3$): δ 170.48, 169.42, 134.36, 133.02, 131.10, 129.78, 126.99, 124.83, 88.67, 64.99, 57.39, 56.04, 43.63, 32.30, 32.06, 31.68, 29.73 (2C), 29.43, 28.01, 26.81, 24.49, 22.87, 14.29, 8.43; ESI-MS (m/z): 456.3 $[M + Na]^+$, 432.2 $[M - H]^-$.

Expression and purification of wild-type and mutants of Na^+-NQR

Site-directed mutants were obtained using the QuikChange Lightning mutagenesis kit (Agilent) as reported before (29). The forward primers used for the mutants in NqrA are as follows: NqrA-Y36A, GCTTGGCGAAGAG**GCC**GTTGGCATGCGTC; NqrA-G38V, GGCGAAGAGTACGTT**GTC**ATGCGTCCTACTATG.

The primers for the mutants in NqrB were reported before (29). Recombinant wild-type Na^+-NQR and mutants were grown in LB medium as reported before (8) in 30-liter fermenters. The expression of the *nqr* operon was induced by adding arabinose. Cells were harvested, washed, and broken in 50 mM Tris-HCl, pH 8, 300 mM NaCl, 10 mM $MgCl_2$ in the presence of DNase and protease inhibitors. Membranes were obtained by ultracentrifugation (100,000 × *g*) and washed with 5 mM imidazole, 300 mM NaCl, 0.05% glycerol. Wild-type and mutant proteins were purified by affinity chromatography as reported before (29).

For preparation of LDAO-washed Na^+-NQR (10), the enzyme stock solution (50 μl) was diluted in a 20-fold volume with a washing buffer (50 mM Tris-HCl, pH 8.0, 1 mM EDTA, 5% glycerol, and 0.05% LDAO), concentrated with a centrifugal filter Amicon Ultra 100 K (Merck-Millipore, Billerica, MA), diluted 20-fold again, and re-concentrated.

Measurement of the electron transfer activity of Na^+-NQR

Steady-state NADH-quinone oxidoreductase activity of purified Na^+-NQR was measured by following the reduction of quinone at 282 nm (ϵ = 14.5 mM^{-1} cm^{-1}) with a Shimadzu UV-3000 instrument at 30 °C (30). The reaction medium (2.5 ml) contained 5% glycerol, 0.05% DDM, 1 mM EDTA, 100 mM NaCl, and 50 mM Tris-HCl, pH 8.0. The final protein concentration was set to 0.9 nM. The reaction was started by adding 100 μM NADH after the incubation of the enzyme with inhibitor and quinone for 5 and 1 min, respectively. The kinetic parameters of quinone reduction were determined by fitting the experimental data to the Michaelis-Menten equation using Prism (version 6, GraphPad, La Jolla, CA).

Photoaffinity labeling of Na^+-NQR by PUQ-3

DDM-purified or LDAO-washed Na^+-NQR was suspended in the reaction buffer (100 mM NaCl, 5% glycerol, and 50 mM Tris-HCl, pH 8.0) containing 0.05% DDM or 0.05% LDAO, respectively. The Na^+-NQR solution (0.9 μM, 30–100 μl) was incubated in a 1.5-ml Eppendorf tube with PUQ-3 (5–10 μM) for 10 min at room temperature. Then, the mixture was irradiated with a long wavelength UV lamp (Black Ray model B-100A, UVP, Upland, CA) for 10 min on ice, positioned 10 cm from the light source. The labeled enzyme sample was denatured with 1% (w/v) SDS at 40 °C for 1 h and conjugated with a fluorescent TAMRA-N_3 tag via Cu^+-catalyzed click chemistry using the

Click-iT Protein reaction buffer kit (Life Technologies, Inc.) according to the manufacturer's instructions (19, 20).

The TAMRA-attached proteins were separated on a Laemmli-type 15% SDS gel containing 6.0 M urea. The migration pattern of fluorescent protein (TAMRA-attached) was visualized using one of two available scanners: a model FLA-5100 (Fuji Film, Tokyo, Japan) or a Typhoon FLA9500 (GE Healthcare, Buckinghamshire, UK) bio-imaging analyzer, in both cases using a 532 nm light source and an LPG emission filter (575 nm). The proteins containing covalently bound FMN (NqrB and NqrC) were visualized using a 473 nm light source and an LPB emission filter (510 nm). MultiGauge (Fuji Film) software was used for data processing. ImageQuant (GE Healthcare) software was used for quantification of fluorescence.

Photoaffinity labeling of Na^+-NQR by [^{125}I]PAD-1 or [^{125}I]PAD-2

The Na^+-NQR solution (0.9 μM, 30 μl) was incubated with [^{125}I]PAD-1 or [^{125}I]PAD and photoirradiated with a UV lamp under the same conditions as those used for the labeling by PUQ-3. The reaction was terminated by addition of an appropriate volume of 4× Laemmli's sample buffer, followed by the separation on a 15% Laemmli-type SDS gel (31) containing 6.0 M urea. The gels were stained with CBB, dried, exposed to an imaging plate (BAS-MS2040, Fuji Film) for 12–24 h, and visualized with the FLA-5100 Bio-Imaging analyzer. The radioactivity of each band was quantified from the digitized data using MultiGauge (Fuji Film) or directly from the gel slices using a γ-counting system (COBLA II, Packard), as described elsewhere (32).

Proteomic analysis

To partially digest the NqrA subunit labeled by PUQ-3, the CBB-stained NqrA band was treated with V8-protease (Roche Applied Science, Penzberg, Germany) in a 15% Tris-EDTA mapping gel using according to the procedures described previously (32–34). The partial digests were characterized by mass spectrometry or N-terminal sequence analysis. For exhaustive digestion, the TAMRA-conjugated NqrA subunit was cleaved by CNBr in 70% aqueous formic acid at 37 °C for 16 h (18). The digests were resolved on a Schägger-type SDS gel (16.5% T, 6% C containing 6.0 M urea, see Ref. 35).

For the analysis of the NqrB subunit labeled by [^{125}I]PAD-1 or [^{125}I]PAD-2, the NqrB subunit was partially isolated by SDS-PAGE and electroelution (19) in a buffer containing 10 mM Tris-HCl, pH 8.0, and 0.025% (w/v) SDS using a model 422 Electro-Eluter (Bio-Rad). The purified subunit was digested with lysyl-endopeptidase (Lys-C, Wako Pure Chemicals, Osaka, Japan) or endoprotease Asp-N (Roche Applied Science) in 50 mM Tris-HCl buffer containing 0.1% SDS or 50 mM NaP_i buffer containing 0.01% SDS, respectively. These digests were separated on a Schägger-type SDS gel.

For the mass spectrometric analysis of proteins, CBB-stained protein bands were digested *in gel* with trypsin (Promega, Fitchburg, WI) in buffer containing 25 mM NH_4HCO_3 at 37 °C overnight. The tryptic digests were desalted with ZipTip (Merck-Millipore) and spotted onto the target plate using α-cyano-4-hydroxycinnamic acid as a matrix (36). A mass spectrometric analysis was conducted using a Bruker Autoflex III Smartbeam MALDI-TOF/TOF instrument (Bruker Daltonics). The mass spectra obtained were analyzed according to previously published procedures (36). N-terminal amino acid residues were examined with a Procise 494 HT protein sequencing system (Applied Life Sciences, Foster City, CA) at the APRO Life Science Institute, Inc. (Tokushima, Japan).

Author contributions—T. I., M. M., B. B., and H. M. designed the research; T. I., M. M., S. N., K. G. M., B. F. C., and M. A. G. K. performed the research; T. I., M. M., Y. K., J. E. M., B. B., and H. M. analyzed the data; T. I., M. M., J. E. M., B. B., and H. M. wrote the paper.

Acknowledgments—We thank Drs. Fumihiko Sato and Kentaro Ifuku (Division of Integrated Life Science, Graduate School of Biostudies, Kyoto University) for allowing us access to their MALDI-TOF MS (Bruker Autoflex III Smartbeam) and for their helpful advice on the experiments, and Dr. Shigenobu Kishino (Division of Applied Life Sciences, Graduate School of Agriculture, Kyoto University) for technical assistance with protein purification. The experiments involving radioisotope techniques were performed at the Radioisotope Research Center, Kyoto University.

References

1. Hayashi, M., Nakayama, Y., and Unemoto, T. (2001) Recent progress in the Na^+-translocating NADH-quinone reductase from the marine *Vibrio alginolyticus*. *Biochim. Biophys. Acta* **1505,** 37–44
2. Juárez, O., and Barquera, B. (2012) Insights into the mechanism of electron transfer and sodium translocation of the Na^+-pumping NADH-quinone oxidoreductase. *Biochim. Biophys. Acta* **1817,** 1823–1832
3. Barquera, B., Zhou, W., Morgan, J. E., and Gennis, R. B. (2002) Riboflavin is a component of the Na^+-pumping NADH-quinone oxidoreductase from *Vibrio cholerae*. *Proc. Natl. Acad. Sci. U.S.A.* **99,** 10322–10324
4. Juárez, O., Morgan, J. E., and Barquera, B. (2009) The electron transfer pathway of the Na^+-pumping NADH:quinone oxidoreductase from *Vibrio cholerae*. *J. Biol. Chem.* **284,** 8963–8972
5. Juárez, O., Morgan, J. E., Nilges, M. J., and Barquera, B. (2010) Energy transducing redox steps of the Na^+-pumping NADH:quinone oxidoreductase from *Vibrio cholerae*. *Proc. Natl. Acad. Sci. U.S.A.* **107,** 12505–12510
6. Bogachev, A. V., Bloch, D. A., Bertsova, Y. V., and Verkhovsky, M. I. (2009) Redox properties of the prosthetic groups of Na^+-translocating NADH: quinone oxidoreductase. 2. Study of the enzyme by optical spectroscopy. *Biochemistry* **48,** 6299–6304
7. Casutt, M. S., Nedielkov, R., Wendelspiess, S., Vossler, S., Gerken, U., Murai, M., Miyoshi, H., Möller, H. M., and Steuber, J. (2011) Localization of ubiquinone-8 in the Na^+-pumping NADH:quinone oxidoreductase from *Vibrio cholerae*. *J. Biol. Chem.* **286,** 40075–40082
8. Juárez, O., Neehaul, Y., Turk, E., Chahboun, N., DeMicco, J. M., Hellwig, P., and Barquera, B. (2012) The role of glycine residues 140 and 141 of subunit B in the functional ubiquinone-binding site of the Na^+-pumping NADH-quinone oxidoreductase from *Vibrio cholerae*. *J. Biol. Chem.* **287,** 25678–25685
9. Nedielkov, R., Steffen, W., Steuber, J., and Möller, H. M. (2013) NMR reveals double occupancy of quinone-type ligands in the catalytic quinone-binding site of the Na^+-translocating NADH:quinone oxidoreductase from *Vibrio cholerae*. *J. Biol. Chem.* **288,** 30597–30606
10. Strickland, M., Juárez, O., Neehaul, Y., Cook, D. A., Barquera, B., and Hellwig, P. (2014) The conformational changes induced by ubiquinone binding in the Na^+-pumping NADH:ubiquinone oxidoreductase (Na^+-NQR) are kinetically controlled by conserved glycines 140 and 141 of the NqrB subunit. *J. Biol. Chem.* **289,** 23723–23733
11. Tuz, K., Mezic, K. G., Xu, T., and Barquera, B., and Juárez, O. (2015) The kinetic reaction mechanism of the *Vibrio cholerae* sodium-dependent NADH dehydrogenase. *J. Biol. Chem.* **290,** 20009–20021

12. Belevich, N. P., Bertsova, Y. V., Verkhovskaya, M. L., Baykov, A. A., and Bogachev, A. V. (2016) Identification of the coupling step in Na^+-translocating NADH:quinone oxidoreductase from real-time kinetics of electron transfer. *Biochim. Biophys. Acta* **1857,** 141–149
13. Steuber, J., Vohl, G., Casutt, M. S., Vorburger, T., Diederichs, K., and Fritz, G. (2014) Structure of the *V. cholerae* Na^+-pumping NADH:quinone oxidoreductase. *Nature* **516,** 62–67
14. Tuz, K., Li, C., Fang, X., Raba, D. A., Liang, P., Minh, D. D., and Juárez, O. (2017) Identification of the catalytic ubiquinone-binding site of *Vibrio cholerae* sodium-dependent NADH dehydrogenase: a novel ubiquinone-binding motif. *J. Biol. Chem.* **292,** 3039–3048
15. Hayashi, M., Shibata, N., Nakayama, Y., Yoshikawa, K., and Unemoto, T. (2002) Korormicin insensitivity in *Vibrio alginolyticus* is correlated with a single point mutation of Gly-140 in the NqrB subunit of the Na^+-translocating NADH-quinone reductase. *Arch. Biochem. Biophys.* **401,** 173–177
16. Yoshikawa, K., Takadera, T., Adachi, K., Nishijima, M., and Sano, H. (1997) Korormicin, a novel antibiotic specifically active against marine Gram-negative bacteria, produced by a marine bacterium. *J. Antibiot.* **50,** 949–953
17. Tebben, J., Motti, C., Tapiolas, D., Thomas-Hall, P., and Harder, T. (2014) A coralline algal-associated bacterium, *Pseudoalteromonas* strain J010, yields five new korormicins and a bromopyrrole, *Mar. Drugs* **12,** 2802–2815
18. Murai, M., Yamashita, T., Senoh, M., Mashimo, Y., Kataoka, M., Kosaka, H., Matsuno-Yagi, A., Yagi, T., and Miyoshi, H. (2010) Characterization of the ubiquinone-binding site in alternative NADH-quinone oxidoreductase of *Saccharomyces cerevisiae* by photoaffinity labeling. *Biochemistry* **49,** 2973–2980
19. Murai, M., Matsunobu, K., Kudo, S., Ifuku, K., Kawamukai, M., and Miyoshi, H. (2014) Identification of the binding site of quinone-head group in mitochondrial Coq10 by photoaffinity labeling. *Biochemistry* **53,** 3995–4003
20. Murai, M., Okuda, A., Yamamoto, T., Shinohara, Y., and Miyoshi, H. (2017) Synthetic ubiquinones specifically bind to mitochondrial voltage-dependent anion channel 1 (VDAC1) in *Saccharomyces cerevisiae* mitochondria. *Biochemistry* **56,** 570–581
21. Wang, Q., Chan, T. R., Hilgraf, R., Fokin, V. V., Sharpless, K. B., and Finn, M. G. (2003) Bioconjugation by copper (I)-catalyzed azide-alkyne [3+2] cycloaddition. *J. Am. Chem. Soc.* **125,** 3192–3193
22. Hayashi, M., Nakayama, Y., Yasui, M., Maeda, M., Furuishi, K., and Unemoto, T. (2001) FMN is covalently attached to a threonine residue in the NqrB and NqrC subunits of Na^+-translocating NADH-quinone reductase from *Vibrio alginolyticus. FEBS Lett.* **488,** 5–8
23. Casutt, M. S., Schlosser, A., Buckel, W., and Steuber, J. (2012) The single NqrB and NqrC subunits in the Na^+-translocating NADH:quinone oxidoreductase (Na^+-NQR) from *Vibrio cholerae* each carry one covalently attached FMN. *Biochim. Biophys. Acta* **1817,** 1817–1822
24. Yoshikawa, K., Nakayama, Y., Hayashi, M., Unemoto, T., and Mochida, K. (1999) Korormicin, an antibiotic specific for gram-negative marine bacteria, strongly inhibits the respiratory chain-linked Na^+-translocating NADH:quinone reductase from the marine *Vibrio alginolyticus. J. Antibiot.* **52,** 182–185
25. Nakayama, Y., Hayashi, M., Yoshikawa, K., Mochida, K., and Unemoto, T. (1999) Inhibitor studies of a new antibiotic, korormicin, 2-*n*-heptyl-4-hydroxyquinoline *N*-oxide and Ag^+ toward the Na^+-translocating NADH-quinone reductase from the marine *Vibrio alginolyticus*. *Biol. Pharm. Bull.* **22,** 1064–1067
26. Huang, L. S., Cobessi, D., Tung, E. Y., and Berry, E. A. (2005) Binding of the respiratory chain inhibitor antimycin to the mitochondrial bc_1 complex: a new crystal structure reveals an altered intramolecular hydrogen-bonding pattern. *J. Mol. Biol.* **351,** 573–597
27. Esser, L., Quinn, B., Li, Y. F., Zhang, M., Elberry, M., Yu, L., Yu, C. A., and Xia, D. (2004) Crystallographic studies of quinol oxidation site inhibitors: a modified classification of inhibitors for the cytochrome bc_1 complex. *J. Mol. Biol.* **341,** 281–302
28. Sakamoto, K., Nomura, K., and Miyoshi, H. (2002) Synthesis and electron-transfer activity of azido-ubiquinone-2. *J. Pestic. Sci.* **17,** 147–149
29. Juárez, O., Athearn, K., Gillespie, P., and Barquera, B. (2009) Acid residues in the transmembrane helices of the Na^+-pumping NADH:quinone oxidoreductase (Na^+-NQR) from *Vibrio cholerae* involved in sodium translocation. *Biochemistry* **48,** 9516–9524
30. Barquera, B., Hellwig, P., Zhou, W., Morgan, J. E., Häse, C. C., Gosink, K. K., Nilges, M., Bruesehoff, P. J., Roth, A., Lancaster, C. R., and Gennis, R. B. (2002) Purification and characterization of the recombinant Na^+-translocating NADH:quinone oxidoreductase from *Vibrio cholerae*. *Biochemistry* **41,** 3781–3789
31. Laemmli, U. K. (1970) Cleavage of structural proteins during the assembly of the head of bacteriophage T4. *Nature* **227,** 680–685
32. Murai, M., Sekiguchi, K., Nishioka, T., and Miyoshi, H. (2009) Characterization of the inhibitor binding site in mitochondrial NADH-ubiquinone oxidoreductase by photoaffinity labeling using a quinazoline-type inhibitor. *Biochemistry* **48,** 688–698
33. Cleveland, D. W., Fischer, S. G., Kirschner, M. W., and Laemmli, U. K. (1977) Peptide mapping by limited proteolysis in sodium dodecyl sulfate and analysis by gel electrophoresis. *J. Biol. Chem.* **252,** 1102–1106
34. Omori, A., Ichinose, S., Kitajima, S., Shimotohno, K. W., Murashima, Y. L., Shimotohno, K., and Seto-Ohshima, A. (2002) Gerbils of a seizure-sensitive strain have a mitochondrial inner membrane protein with different isoelectric points from those of a seizure-resistant strain. *Electrophoresis* **23,** 4167–4174
35. Schägger, H. (2006) Tricine-SDS-PAGE. *Nat. Protoc.* **1,** 16–22
36. Shiraishi, Y., Murai, M., Sakiyama, N., Ifuku, K., and Miyoshi, H. (2012) Fenpyroximate binds to the interface between PSST and 49-kDa subunits in mitochondrial NADH-ubiquinone oxidoreductase. *Biochemistry* **51,** 1953–1963